RENATO DICHETTI DOS REIS LISBOA

AVALIAÇÃO DIAGNÓSTICA DA TOMOGRAFIA DE COERÊNCIA ÓPTICA NO GLAUCOMA E SUA APLICAÇÃO CLÍNICA

Tese apresentada à Universidade Federal de São Paulo – Escola Paulista de Medicina – para obtenção do Título de Doutor em Ciências pelo programa de Pós-graduação em Oftalmologia

SÃO PAULO
2014

RENATO DICHETTI DOS REIS LISBOA

AVALIAÇÃO DIAGNÓSTICA DA TOMOGRAFIA DE COERÊNCIA ÓPTICA NO GLAUCOMA E SUA APLICAÇÃO CLÍNICA

Tese apresentada à Universidade Federal de São Paulo – Escola Paulista de Medicina – para obtenção do Título de Doutor em Ciências pelo programa de Pós-graduação em Oftalmologia

Orientador:
Prof. Dr. Augusto Paranhos Jr.
Coorientador:
Prof. Dr. Felipe Andrade Medeiros

SÃO PAULO
2014

Lisboa, Renato Dichetti dos Reis

Avaliação diagnóstica da tomografia de coerência óptica no glaucoma e sua aplicação clínica. São Paulo, 2014./Renato Dichetti dos Reis Lisboa. -- São Paulo, 2014

xi, 63f.

Tese (Doutorado) - Universidade Federal de São Paulo. Escola Paulista de Medicina. Programa de Pós-graduação em Oftalmologia.

Título em inglês: Diagnostic evaluation of the spectral domain optical coherence tomography in the preperimetric glaucoma and its clinical application.

1. Glaucoma. 2. Oftalmologia. 3.Diagnóstico. 4. Células ganglionares da retina. 5. Disco óptico. 6. Tomografia

UNIVERSIDADE FEDERAL DE SÃO PAULO
ESCOLA PAULISTA DE MEDICINA
DEPARTAMENTO DE OFTALMOLOGIA

Chefe do Departamento:
Profa. Dra. Denise de Freitas

Coordenador do Curso de Pós-graduação:
Prof. Dr. Mauro Silveira de Queiroz Campos

RENATO DICHETTI DOS REIS LISBOA

AVALIAÇÃO DIAGNÓSTICA DA TOMOGRAFIA DE COERÊNCIA ÓPTICA NO GLAUCOMA E SUA APLICAÇÃO CLÍNICA

Presidente da Banca:
Prof. Dr. Augusto Paranhos Jr.

Banca Examinadora:
Dr. Lisandro Massanori Sakata
Dra. Luciana Pereira Malta de Alencar
Prof. Dr. Paulo Augusto de Arruda Mello - Banca Prévia
Dr. Roberto Murad Vessani

Suplentes:
Dr. Sergio Henrique Teixeira
Prof. Dr. Geraldo Vicente de Almeida

DEDICATÓRIAS

À Maria, que veio de tão longe para estar tão perto nos incontáveis momentos de alegrias ao meu lado.

Aos meus pais, pelo amor, apoio incondicional aos meus estudos e exemplo de trabalho.

AGRADECIMENTOS

“Make friends with pain, and you will never be alone”

Ken Chlouber
Minerador do Colorado e criador da Leadville Trail 100

Ao Professor Felipe A. Medeiros, pelo exemplo de perfeccionismo, dedicação e paciência.

Ao Professor Augusto Paranhos Jr, pela amizade e exemplo como profissional e educador.

Ao Professor Paulo Augusto de Arruda Mello, pelo incentivo à pesquisa desde a graduação até o doutorado e pelo exemplo de cavalheirismo.

Ao Dr. Mauro Toledo Leite e ao tecnólogo Ali Tafreshi, pela amizade e ajuda fundamentais para realização desta tese.

Aos Drs. Sérgio Henrique Teixeira, Ednajar Macedo, André Luiz, Luiz Alberto, Ivan Tavares, pelo exemplo como profissionais e ensinamentos durante a residência e especialização.

Ao Dr. Daniel Meira Freitas, pela amizade e proveitosas discussões sobre projetos científicos.

Ao Professor Robert Weinreb, pelo exemplo de iniciativa e perseverança.

À Professora Linda Zangwill, pelo exemplo de organização.

Aos colegas do Glaucoma na Escola Paulista de Medicina, pelos incontáveis ensinamentos e amizade.

LISTA DE ABREVIATURAS E SÍMBOLOS

CFNR	Camada de fibras nervosas da retina
CNO	Cabeça do nervo óptico
CSLO	Oftalmoscópio confocal de varredura a laser
et al.	e outros, da expressão latina *et alii*
P(D)	Probabilidade de doença pré-teste
P(T|D)	Probabilidade do resultado do teste na presença de doença
$P(T\|\overline{D})$	Probabilidade do resultado do teste na ausência de doença
$\frac{P(T\|D)}{P(T\|\overline{D})}$	Razão de verossimilhança
P(D|T)	Probabilidade de doença após o conhecimento do resultado do teste
ROC	Receiver operating characteristic
SD-OCT	Tomógrafo de coerência óptica de domínio espectral

RESUMO

Objetivo: Este estudo foi realizado para caracterizar o dano estrutural no glaucoma pré-perimétrico com o tomógrafo de coerência óptica de domínio espectral (SD-OCT) e foi dividido em em três fases: 1) avaliação da capacidade do SD-OCT em detectar o dano glaucomatoso pré-perimétrico por meio de medidas da espessura da camada de fibras nervosas da retina (CFNR) e compará-la à capacidade diagnóstica do oftalmoscópio confocal de varredura a laser (CSLO); 2) comparação da capacidade de detecção do dano glaucomatoso pré-perimétrico de medidas da espessura da CFNR, medidas topográficas da cabeça do nervo óptico (CNO) e medidas da espessura macular fornecidas pelo SD-OCT e 3) estimativa da razão de verossimilhança para valores contínuos da espessura da CFNR fornecidos pelo SD-OCT em uma coorte de pacientes com glaucomas pré-perimétrico e perimétrico. **Métodos:** Na primeira fase foram incluídos 134 olhos de 88 suspeitos de glaucoma, fundamentado na aparência da CNO. Todos os pacientes tinham campo visual normal e foram classificados como possuidores ou não de glaucoma pré-perimétrico com base na presença de dano glaucomatoso progressivo anterior aos exames de imagem. Na segunda fase, foram incluídos 142 olhos de 91 pacientes suspeitos de glaucoma, como descrito na primeira fase. Na terceira fase foram incluídos 262 olhos de 187 pacientes com glaucoma e 190 olhos de 100 indivíduos controle. Olhos com danos glaucomatoso perimétrico e pré-perimétrico foram incluídos. Uma metodologia que estima as tangentes da curva ROC foi utilizada para calcular razões de verossimilhança para valores contínuos da espessura da CFNR. **Resultados:** Na primeira fase, o parâmetro da CFNR obtido com o SD-OCT com maior área abaixo da curva ROC (receiver operating characteristic) foi a espessura temporal superior. Este parâmetro apresentou uma área abaixo da curva ROC maior do que o melhor parâmetro do CSLO (área da rima) (0.88 vs. 0.72; P = 0.008). Na segunda fase, o melhor parâmetro da CFNR (espessura média da CFNR) apresentou uma área abaixo da curva ROC maior que o melhor parâmetro topográfico da CNO (relação escavação-disco vertical) (0.89 vs. 0.74; P = 0.007) e o melhor parâmetro macular (espessura média do

complexo de células ganglionares) (0.89 vs. 0.79; *P* = 0.015). Na terceira fase, razões de verossimilhança para valores contínuos da espessura da CFNR foram calculados. Um nomograma de Fagan modificado foi proposto para auxiliar no cálculo da probabilidade pós-teste de glaucoma. **Conclusões:** As medidas da CFNR apresentaram boa capacidade em detectar dano glaucomatoso pré-perimétrico, apresentando áreas abaixo da curva ROC superiores às medidas da CNO e da mácula. O nomograma de Fagan modificado proposto pode ser utilizado de forma simples na prática diária em glaucoma com o objetivo de agregar a informação diagnóstica fornecida pela espessura da CFNR.

ABSTRACT

Purpose: This study was conducted to characterize the structural damage in preperimetric glaucoma and was divided in three steps with the following purposes: 1) evaluate the capability for detection of preperimetric glaucomatous damage of the retinal nerve fiber layer (RNFL) obtained with the spectral domain optical coherence tomography (SD-OCT) and compare it with the performance of the confocal scanning laser ophthalmoscopy (CSLO); 2) compare the diagnostic accuracy for preperimetric glaucomatous damage of RNFL thickness measurements, topographic measurements of the optic nerve head (ONH) and macular measurements obtained with the SD-OCT; and 3) estimate likelihood ratios for continuous values of RNFL thickness provided by the SD-OCT in a cohort of patients with preperimetric or perimetric glaucoma. **Methods:** In the first step 134 eyes of 88 glaucoma suspects based on the appearance of the optic disc were included. All patients had normal visual fields at the time of the imaging and were classified as preperimetric glaucomatous patients on the basis of history of documented stereophotographic evidence of progressive glaucomatous damage before the imaging sessions. In the second step 142 eyes from 91 patients suspected of having the disease as described previously were included. The third step included 262 eyes of 187 patients with glaucoma and 190 eyes of 100 control subjects. Eyes with perimetric and preperimetric glaucomatous damage were included. A methodology that estimates the tangents of the ROC curve was applied in order to calculate likelihood ratios for continuous values of RNFL thicknesses. **Results:** In the first step, the RNFL parameter obtained with the SD-OCT with largest area under the ROC (receiver operating characteristic) curve was the temporal superior RNFL thickness. This parameter had a larger area under the ROC curve then the best performing CSLO parameter (rim area) (0.88 vs. 0.72; P = 0.008). In the second step, the best RNFL parameter (RNFL average thickness) had a larger area under the

ROC curve than the best ONH parameter (vertical cup-to-disc ratio) (0.89 vs. 0.74; *P* = 0.007) and the best macular parameter (ganglion cell average thickness) (0.89 vs. 0.79; *P* = 0.015). In the third step, likelihood ratios for continuous values of RNFL thickness could be calculated. A modified Fagan nomogram was proposed to assist the calculation of the posttest probability of the disease. **Conclusions:** RNFL thickness measurements provided by the SD-OCT performed well in detecting preperimetric glaucomatous damage. RNFL measurements performed better than topographic ONH measurements and macular measurements. Diagnostic information obtained with RNFL measurements can be included in the decision-making process in the clinical practice using the modified Fagan nomogram.

SUMÁRIO

1. INTRODUÇÃO

"Não importa quão duro o passado, você sempre pode começar de novo."

Sidarta Gautama, o Buda
Guia Espiritual

Glaucoma é uma neuropatia óptica com mudanças estruturais características na cabeça do nervo óptico (CNO), frequentemente acompanhada por mudanças correspondentes no campo visual.[1] As características demográficas e clínicas associadas a essa doença foram amplamente descritas na literatura médica.[2] Contudo, devido à grande variabilidade dos achados clínicos, oftalmologistas frequentemente encontram dificuldades em diagnosticá-la de forma segura. Diante da suspeita diagnóstica, a avaliação oftalmológica pode ser complementada com exames de imagem.[3] Os resultados destes exames auxiliam a decidir se a neuropatia óptica glaucomatosa está ou não presente.

A tomografia de coerência óptica de domínio espectral (SD-OCT, do inglês *spectral domain optical coherence tomography*) representa uma evolução da tomografia de coerência óptica de domínio temporal (TD-OCT, do inglês *time domain optical coherence tomography*), potencialmente superior na avaliação do dano estrutural glaucomatoso.[4,5] Os princípios físicos aplicados nas duas tecnologias são semelhantes. Em ambas uma luz superluminescente é aplicada sobre tecidos oculares com o objetivo de analisar a luz refletida e assim obter estimativas das medidas das estruturas estudadas. O que as diferencia é a análise da luz refletida pelos tecidos. Enquanto o TD-OCT estima as medidas através da movimentação de um espelho de referência, o SD-OCT utiliza um espectofotômetro. Desta forma, o SD-OCT é capaz de obter mais cortes transversais com maior resolução em um mesmo período de tempo. O maior número de cortes transversais proporciona maior detalhamento das estruturas,[6] bem como diminuição no número de artefatos e maior reprodutibilidade.[7] Dois diferentes SD-OCTs foram utilizados para a coleta dos dados nos artigos científicos incluídos nesta tese. O Spectralis é fabricado pela Heidelberg

Engineering, situada em Carlsbad, California, Estados Unidos. O RTVue é fabricado pela Optovue, situada em Fremont, California, Estados Unidos.

Diversos estudos anteriores avaliaram a capacidade do SD-OCT identificar o dano glaucomatoso.[8-26] Não obstante a importância destes estudos para uma avaliação inicial desta tecnologia, a estimativa de sua capacidade diagnóstica pode não ser a ideal para uso na prática clínica. Nestes estudos, a acurácia diagnóstica reportada para o SD-OCT baseou-se na capacidade do instrumento separar pacientes glaucomatosos com dano de campo visual de indivíduos sadios. Contudo, sua metodologia não reflete o cenário encontrado na prática clínica, onde a presença de alteração no campo visual em um paciente com achados biomicroscópicos de glaucoma encerra o diagnóstico, dispensando assim a realização de exames complementares de imagem. Na realidade, quando se trata de glaucoma, exames de imagem agregam informação diagnóstica em casos em que há incompatibilidade dos achados biomicroscópicos com os resultados dos campos visuais. Em outras palavras, para fins diagnósticos, exames de imagem são úteis na presença de achados glaucomatosos à biomicroscopia e campos visuais normais.

Outra importante limitação dos estudos de imagem está na forma de reportar a capacidade diagnóstica dos instrumentos. Sensibilidade, especificidade e área abaixo das curvas ROC (do inglês, *receiver operating characteristic*) são tradicionalmente utilizadas. Contudo, esses índices não podem ser diretamente aplicados para modificar a probabilidade inicial da doença em uma nova probabilidade mais conclusiva. *Likelihood ratio*, que em português corresponderia à razão de verossimilhança, pode ser utilizada diretamente para modificar a probabilidade inicial (probabilidade pré-teste) em uma probabilidade final mais precisa (probabilidade pós-teste). Publicações anteriores propuseram que o uso da razão de verossimilhança é a melhor maneira de agregar os resultados de um teste diagnóstico na prática clínica.[27] Apesar de alguns destes estudos sobre glaucoma terem reportado razões de verossimilhança,[11,28-30] os resultados dos testes foram arbitrariamente categorizados em normal ou anormal, de acordo com pontos de corte predeterminados. A categorização de

resultados contínuos pode resultar em importante perda de informação, principalmente quando estes resultados estão próximos do ponto de corte determinado.[31-35]

Com o objetivo de facilitar a aplicação da razão de verossimilhança à prática clínica Fagan propôs um nomograma (Figura).[36] Este nomograma pode ser utilizado para calcular diretamente a probabilidade pós-teste a partir da probabilidade pré-teste e da razão de verossimilhança. Nesta Figura, *P(D)* representa a probabilidade inicial da doença, ou probabilidade pré-teste. Esta probabilidade é calculada com base na história e achados clínicos pelo oftalmologista antes da realização do exame complementar. As razões de verossimilhança estão representadas na coluna do meio da Figura. A razão de verossimilhança representa a razão entre duas probabilidades. *P(T|D)* é a probabilidade do resultado do teste se o paciente tem a doença, enquanto $P(T|\overline{D})$ representa a probabilidade do resultado do teste se o paciente não tem a doença. Ao traçar uma linha reta a partir da probabilidade pré-teste *P(D)* que atravessa a razão de verossimilhança fornecida pelo resultado do teste diagnóstico podemos calcular a probabilidade pós-teste de doença *P(D|T).*

Para que possamos melhor avaliar as informações fornecidas pelo SD-OCT, em um contexto que se assemelhe à prática clínica, é necessário estudar a sua capacidade diagnóstica em pacientes suspeitos de glaucoma. Também é necessário avaliar a relação dos resultados contínuos fornecidos pelo instrumento e a razão de verossimilhança. Conhecendo as razões de verossimilhança correspondentes aos valores contínuos da CFNR, poderemos propor um nomograma de Fagan modificado. Este nomograma teria sua coluna do meio representada por valores de espessura da CFNR e poderia ser diretamente utilizado na prática clínica do glaucoma.

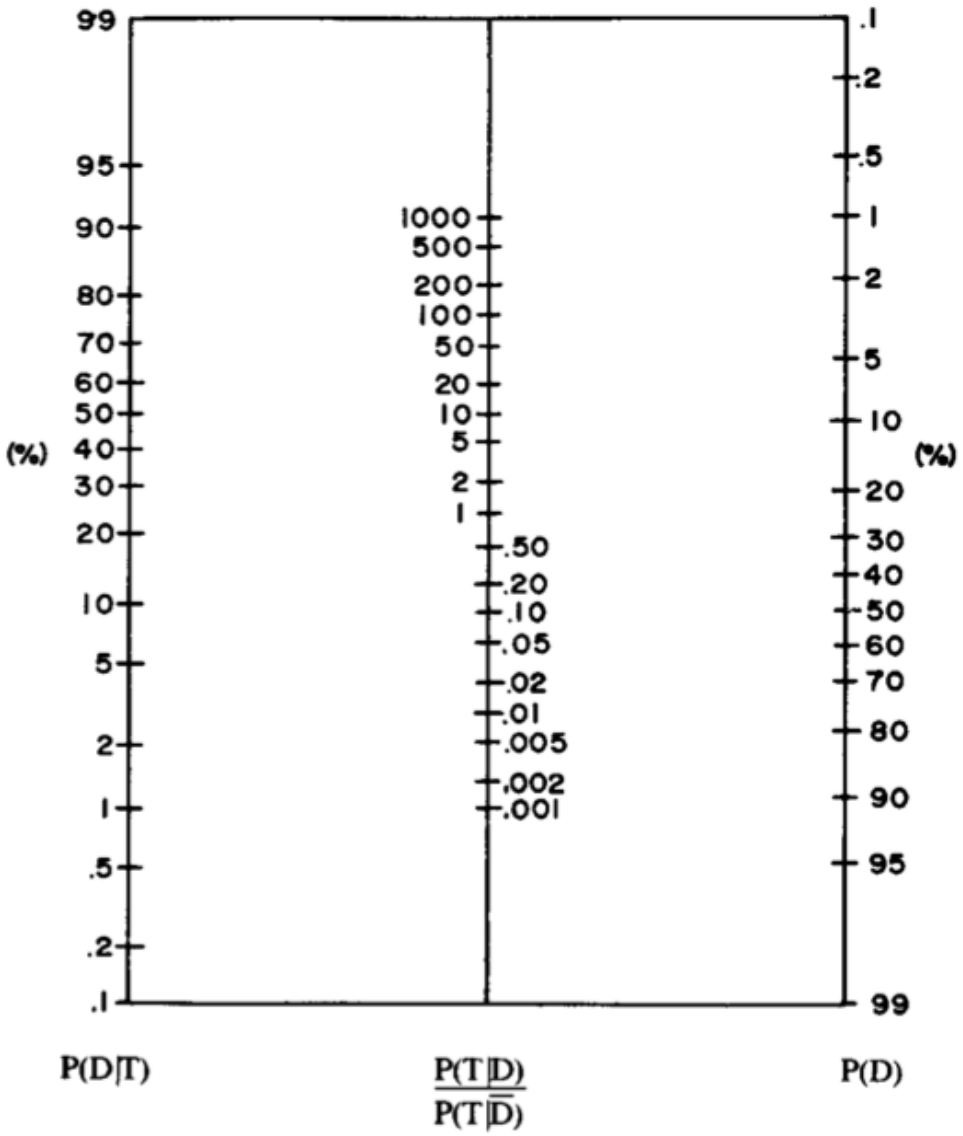

Figura – Nomograma de Fagan. *P(D)* representa a probabilidade de doença pré-teste. $\frac{P(T \mid D)}{P(T \mid \overline{D})}$ representa a razão de verossimilhança e *P(D|T)* a probabilidade de doença após o conhecimento do resultado do teste diagnóstico. Uma linha desenhada a partir de *P(D)* através da razão de verossimilhança na coluna do meio fornecerá a probabilidade pós-teste *P(D|T).*

1.1. Objetivos

“Um bom arqueiro não é conhecido por suas flechas,
mas por seus alvos”

T. Fuller
Eclesiástico e historiador britânico

1. Avaliar a capacidade das medidas de espessura da CFNR fornecidas pelo SD-OCT para detectar dano glaucomatoso pré-perimétrico e compará-las à capacidade diagnóstica das medidas topográficas da CNO fornecidas pelo oftalmoscópio confocal de varredura a laser (CSLO; do inglês, *confocal scanning laser ophthalmoscopy*).

2. Comparar a acurácia diagnóstica das medidas de espessura da CFNR, medidas topográficas da CNO e medidas da espessura macular fornecidas pelo SD-OCT para detecção do glaucoma pré-perimétrico em pacientes suspeitos de glaucoma.

3. Estimar razões de verossimilhança para valores contínuos da espessura da CFNR e propor um nomograma de Fagan modificado a ser utilizado na prática clínica do glaucoma.

2. ARTIGOS

2.1. Diagnosing Preperimetric Glaucoma with Spectral Domain Optical Coherence Tomography

Renato Lisboa, MD; Mauro T. Leite, MD; Linda M. Zangwill, PhD; Ali Tafreshi, BS; Robert N. Weinreb, MD; Felipe A. Medeiros, MD, PhD.

Ophthalmology, 2012 Nov; 119(11):2261-69

Diagnosing Preperimetric Glaucoma with Spectral Domain Optical Coherence Tomography

Renato Lisboa, MD,[1,2] Mauro T. Leite, MD,[2] Linda M. Zangwill, PhD,[1] Ali Tafreshi, BS,[1] Robert N. Weinreb, MD,[1] Felipe A. Medeiros, MD, PhD[1]

Purpose: To evaluate the diagnostic accuracy of spectral domain optical coherence tomography (SD-OCT) for detection of preperimetric glaucoma and compare it with the performance of confocal scanning laser ophthalmoscopy (CSLO).

Design: Cohort study.

Participants: A cohort of 134 eyes of 88 glaucoma suspects based on the appearance of the optic disc.

Methods: Patients were recruited from the Diagnostic Innovations in Glaucoma Study (DIGS). All eyes underwent retinal nerve fiber layer (RNFL) imaging with Spectralis SD-OCT (Heidelberg Engineering, Carlsbad, CA) and topographic imaging with Heidelberg Retinal Tomograph III (HRT-III) (Heidelberg Engineering) CSLO within 6 months of each other. All patients had normal visual fields at the time of imaging and were classified on the basis of history of documented stereophotographic evidence of progressive glaucomatous change in the appearance of the optic nerve occurring before the imaging sessions.

Main Outcome Measures: Areas under the receiver operating characteristic curves (AUCs) were calculated to summarize diagnostic accuracies of the SD-OCT and CSLO. Likelihood ratios (LRs) were reported using the diagnostic categorization provided by each instrument after comparison to its normative database.

Results: Forty-eight eyes of 42 patients had evidence of progressive glaucomatous change and were included in the preperimetric glaucoma group. Eighty-six eyes of 46 patients without any evidence of progressive glaucomatous change followed untreated for an average of 14.0±3.6 years were included in the control group. The parameter with the largest AUC obtained with the SD-OCT was the temporal superior RNFL thickness (0.88±0.03), followed by global RNFL thickness (0.86±0.03) and temporal inferior RNFL thickness (0.81±0.04). The parameter with the largest AUC obtained with the CSLO was rim area (0.72±0.05), followed by rim volume (0.71±0.05) and linear cup-to-disk ratio (0.66±0.05). Temporal superior RNFL average thickness measured by SD-OCT performed significantly better than rim area measurements from CSLO (0.88 vs. 0.72; $P=0.008$). Outside normal limits results for SD-OCT parameters were associated with strongly positive LRs.

Conclusions: The RNFL assessment with SD-OCT performed well in detecting preperimetric glaucomatous damage in a cohort of glaucoma suspects and had a better performance than CSLO.

Financial Disclosure(s): Proprietary or commercial disclosure may be found after the references.
Ophthalmology 2012;119:2261–2269 © 2012 by the American Academy of Ophthalmology.

Clinicians are frequently faced with the challenge of diagnosing glaucoma in patients who present with optic discs that have suspicious findings for the disease, such as apparent enlarged cupping or neuroretinal rim thinning, but in whom clinical examination at the slit-lamp or using optic disc photographs is inconclusive. In the presence of normal visual field tests, clinicians may complement their evaluation by ordering additional diagnostic tests, such as quantitative evaluation of the optic nerve or retinal nerve fiber layer (RNFL) with imaging instruments. The results obtained from imaging evaluation can assist clinicians in deciding whether preperimetric glaucomatous optic neuropathy is present and in establishing treatment and follow-up plans.

The introduction of spectral domain optical coherence tomography (SD-OCT) has resulted in improved imaging resolution and reproducibility compared with previous versions of this technology,[1,2] offering the potential for improved assessment of structural damage in glaucoma. Although several studies have evaluated the diagnostic accuracy of imaging devices in glaucoma, the design has not replicated their situation in which these tests are used in clinical practice. Most studies have been performed by comparing the ability of imaging devices to discriminate patients with confirmed glaucomatous visual field loss from healthy individuals in a cross-sectional design.[3–21] However, it should be obvious that the presence of visual field loss by itself would obviate the need for using an imaging instrument to diagnose the disease in clinical practice. In fact, a clinician is most interested in the ability of a test to provide additional information that can be helpful for a patient who presents suspicious findings for the disease, as described previously.

The conduct of studies evaluating glaucoma suspects and detecting preperimetric damage has been limited by the

ISSN 0161-6420/12/$–see front matter
http://dx.doi.org/10.1016/j.ophtha.2012.06.009

inexistence of a perfect reference standard that could be used to diagnose disease at a single point in time without relying on visual fields. However, longitudinal follow-up can be used to evaluate the existence of progressive structural damage, which would then confirm the diagnosis.[22–25] The final diagnosis based on longitudinal follow-up can then be used as a reference standard with which the results of the imaging instruments are to be compared.

This study evaluates the diagnostic accuracy of RNFL with Spectralis SD-OCT (Heidelberg Engineering, Carlsbad, CA) for the detection of preperimetric glaucomatous damage in glaucoma suspects. In addition, we compared the diagnostic ability of the SD-OCT technology with the diagnostic ability of optic disc topographic measurements obtained by confocal scanning laser ophthalmoscopy (CSLO). We used longitudinal information to establish the final diagnosis in these patients and as a reference standard for comparison of results.

Materials and Methods

Participants

This was an observational cohort study that included patients recruited from the Diagnostic Innovations in Glaucoma Study (DIGS) conducted at the Hamilton Glaucoma Center (University of California, San Diego). As part of DIGS, participants were prospectively evaluated according to a pre-established protocol that included visits with a comprehensive clinical examination and several imaging and functional tests. All participants who met the inclusion criteria described next were enrolled, and all data were entered in a computer database. Informed consent was obtained from all participants. The University of California San Diego Human Subjects Committee approved all protocols, and methods described attended to the tenets of the Declaration of Helsinki.

Each subject underwent a comprehensive ophthalmic examination, including review of medical history, best-corrected visual acuity, slit-lamp biomicroscopy, intraocular pressure measurement using Goldmann applanation tonometry, gonioscopy, dilated fundoscopy examination using a 78-diopter (D) lens, stereoscopic optic disc photography, and standard automated perimetry with 24–2 Swedish Interactive Threshold Algorithm (Carl Zeiss Meditec, Inc., Dublin, CA).

To be included, subjects had to have best-corrected visual acuity of 20/40 or better, spherical refraction less than ±5.0 D, cylinder correction less than 3.0 D, and open angle with gonioscopy. Subjects with coexisting retinal disease, uveitis, or nonglaucomatous optic disc neuropathy were excluded from the study.

A cohort of glaucoma suspects was selected from our DIGS database. These participants were selected on the basis of the presence of suspicious appearance of the optic nerve from cross-sectional evaluations of stereophotographs at the time of imaging by 2 independent masked graders. A third experienced grader reviewed the stereophotographs in case of disagreement. Features characteristic of suspicious glaucomatous appearance of the optic disc were neuroretinal rim thinning, cupping, or suspicious RNFL defects. All participants had a normal standard automated perimetry visual field result at the time of imaging. A normal visual field was defined as a mean deviation and pattern standard deviation within 95% confidence limits and a glaucoma hemifield test result within normal limits. In addition, participants did not have evidence of repeatable glaucomatous visual field loss before the date of their examination with imaging instruments. All participants had been followed for at least 5 years before their imaging session.

These participants were then classified on the basis of a history of documented evidence of progressive glaucomatous change in the appearance of the optic disc occurring before the imaging sessions. Patients with documented evidence of progressive glaucomatous nerve damage at any time before both imaging sessions with SD-OCT and CSLO were considered as having preperimetric glaucoma. Progressive glaucomatous change in the appearance of the optic disc was assessed by simultaneous stereoscopic photographs (TRC-SS, Topcon Instrument Corp. of America, Paramus, NJ). Stereoscopic sets of slides were examined using a stereoscopic viewer (Asahi, Pentax, Tokyo, Japan). The stereophotographs were evaluated by 2 experienced graders, and each was masked to the subject's identity, to other test results, and to the chronological sequence of the photographs. For inclusion, stereophotographs needed to be graded adequate or better. Definition of change was based on focal or diffuse thinning of the neuroretinal rim, increased excavation, or enlargement of the RNFL defects. Changes in rim color, presence of disc hemorrhages, or progressive parapapillary atrophy were not sufficient for characterization of progression. Discrepancies between the 2 graders were resolved by consensus or adjudication of a third experienced grader.

A total of 48 eyes of 42 participants with progressive optic disc damage and no visual field loss were included in the preperimetric glaucoma group. These subjects were followed for an average of 14.9±4.2 years.

A total of 86 eyes of 46 patients followed untreated for 14.0±3.6 years without any evidence of progressive change in the appearance of the optic disc or visual field loss were used as the control group.

Instrumentation

The Spectralis SD-OCT (software v. 5.3.3.0) was used to obtain RNFL thickness measurements. Details of its operation have been published.[26] The high-resolution protocol was used, obtaining 1536 A-scans from a 3.45-mm circle centered at the optic disc, providing an axial resolution of 3.9 μm and a lateral resolution of 6 μm. The examiner was required to manually place the scan around the optic disc. To increase the image quality, the Spectralis SD-OCT includes an automatic real-time function that gathers multiple frames (B-scans). The images were then averaged for noise reduction. The standard deviation of the signal-to-noise ratio was available to the examiner, enabling the assessment of the signal's acceptability. The quality scores ranges from 0 dB (poor) to 40 dB (excellent). To be included, all images were reviewed by experienced staff of the Imaging Data Evaluation and Assessment Center for noncentered scans, accurate segmentation, and a signal strength >15 dB. The parapapillary RNFL thickness sectors evaluated in this study were temporal quadrant (316–45 degrees), temporal superior quadrant (46–90 degrees), nasal superior quadrant (91–135 degrees), nasal quadrant (136–225 degrees), nasal inferior quadrant (226–270 degrees), and temporal inferior quadrant (271–315 degrees).

For each parameter, the Spectralis SD-OCT software provides a classification (within normal limits, borderline, and outside normal limits) based on the comparison with an internal normative database of 201 healthy eyes of Caucasian patients. The parameter is classified as within normal limits if its value falls within the 95% confidence interval (CI) of the healthy, age-matched population. A borderline result indicates that the value is between the 99% and 95% CI, and an outside normal limits result indicates that the value is less than the 99% CI. This classification is provided in the Spectralis SD-OCT printout using a color-coded pattern where within normal limits, borderline, and outside normal limits

results are represented in green, yellow, and red, respectively. The software also provides an overall classification. A normal overall classification requires all sectors and the global thickness to be within normal limits. A borderline result occurs when at least 1 sector or the global thickness is classified as borderline, and an outside normal limit result is provided if at least 1 sector or the global thickness is outside normal limits. Likelihood ratios (LRs) were calculated for each parameter and each possible diagnostic categorization (within normal limits, borderline, and outside normal limits), as provided by the Spectralis SD-OCT software.

The Heidelberg Retinal Tomograph III (HRT-III) (Heidelberg Explorer Software v. 1.5.10.0, Heidelberg Engineering) was used to acquire CSLO images in the study. It uses confocal scanning laser principles to obtain a 3-dimensional topographic image of the optic nerve. For each patient, 3 topographic images were obtained, combined, and automatically aligned to make a single mean for topography for analysis. Magnification errors were corrected using patients' corneal curvature measurements. An experienced examiner outlined the optic nerve margin on the mean topographic image while viewing stereoscopic photographs of the optic disc. Good images required a focused reflectance image with a standard deviation not greater than 50 μm, as determined by experienced reviewers from the Imaging Data Evaluation and Assessment Center.

Topographic parameters provided by the HRT-III software and investigated in this study were rim area, rim volume, linear cup-to-disk ratio, cup-to-disk area ratio, rim-to-disk area ratio, RNFL cross-sectional area, mean RNFL thickness, cup area, cup volume, and mean cup depth. The global glaucoma probability score (GPS) was also evaluated as a diagnostic variable in this study. This score uses an automated analysis for the detection of glaucomatous damage that does not require the user to draw a contour line around the optic disc and does not use a reference plane. It is based on a 3-dimensional model of the entire topographic image, including the optic disc and surrounding peripapillary RNFL. The development of this parameter is based on the work of Swindale et al.[27]

The software for the HRT-III also incorporates the Moorfields Regression Analysis (MRA),[28] which compares the patient's rim area with a predicted rim area for a given disc area and age, based on confidence limits of a regression analysis derived from 627 normal patients (452 Caucasians, 111 of African origin, and 64 Indians). Each sector and the global rim area are classified as within normal limits if the measurement is within the 95% CI, borderline if the measurements are between the 99.9% and 95% CI, and outside normal limits if the measurements is lower than the 99.9% CI. The MRA also provides an overall classification. A normal overall classification requires all sectors and the global rim area to be within normal limits. A borderline result occurs when at least 1 sector or the global rim area is classified as borderline, and an outside normal limit result is provided if at least 1 sector or the global rim area is outside normal limits. The LRs were calculated for each possible diagnostic categorization (within normal limits, borderline, and outside normal limits) of the global and sectoral results and for the overall classification of the MRA.

Statistical Analysis

Descriptive statistics included mean and standard deviation for normally distributed variables and median, first quartile, and third quartile for non-normally distributed variables.

Areas under the receiver operating characteristic curves (AUCs) were calculated to summarize the diagnostic accuracy for each parameter. An AUC equal to 1 represents perfect discrimination, whereas an AUC of 0.5 represents chance discrimination. The pairwise comparison of the AUCs was performed for each parameter using a method proposed by Dodd and Pepe.[29] A bootstrap resampling procedure (n = 1000 resamples) was used to derive the CIs.[30] Sensitivity at fixed specificities of 80% and 95% were also reported for each parameter of each instrument. To account for potential correlation between eyes, the cluster of the data for the study subject were considered as the unit of resampling when calculating standard errors. This procedure has been used to adjust for the presence of multiple correlated measurements of the same unit.[30,31]

Diagnostic categorization (within normal limits, borderline, or outside normal limits) provided by each instrument after comparison with its normative database was used to calculate LRs. The LR is defined as the probability of a given test result in those with disease divided by the probability of the same test result in those without disease.[32,33] Once determined, an LR can be directly incorporated into the calculation of post-test probability of disease by using the formulation of the Bayes' theorem.[34] The LR for a given test result indicates how much that result will increase or decrease the pretest odds of disease. Application of LRs in the interpretation of results of imaging instruments for glaucoma diagnosis has been detailed.[6,24] A value of 1 means that the test provides no additional information, and ratios more or less than 1 increase or decrease the likelihood of disease, respectively.

A classification of impact of LRs of various magnitudes on post-test probability of disease has been suggested and was used in our study.[33] According to this classification, LRs greater than 10 or less than 0.1 would be associated with large effects on post-test probability, LRs from 5 to 10 or from 0.1 to 0.2 would be associated with moderate effects, LRs from 2 to 5 or from 0.2 to 0.5 would be associated with small effects, and LRs closer to 1 would be insignificant. The CIs of 95% for LRs were calculated according to the method proposed by Simel et al.[35]

All statistical analyses were performed with commercially available software (Stata v. 11, StataCorp, College Station, TX). The alpha level (type I error) was set at 0.05.

Results

Table 1 shows demographic and clinical characteristics for the eyes included in the study. No difference in age, sex, or ancestry was found between the groups.

Table 2 shows mean values of SD-OCT parameters in the glaucoma and control groups. Glaucomatous eyes had, on average, significantly thinner RNFL measurements compared with the control group. The parameters with the largest AUCs were temporal superior thickness (0.88±0.03), global thickness (0.86±0.03), and temporal inferior thickness (0.81±0.04). Figure 1 shows receiver operating characteristic (ROC) curves for these parameters.

Table 3 presents LRs with 95% CIs for the Spectralis SD-OCT after comparison with the instrument's normative database. For all parameters, an outside normal limits result was associated with large effects on the post-test probability of disease, except for nasal superior thickness, which was associated with moderate effects. The effect on post-test probability for borderline results ranged from insignificant to large. Within normal limits results were associated with small to insignificant effects on post-test probability of disease. An outside normal limit result in the overall Spectralis SD-OCT classification was associated with a large effect on the post-test probability (LR = 50.16), whereas a borderline result was associated with an insignificant (LR = 1.05) effect and a within normal limits result was associated with small (LR = 0.26) effect on the post-test probability of disease.

Table 4 shows the mean values of CSLO parameters in the glaucoma and control groups. Statistically significant differences between the glaucoma and control groups were found for most parameters, except for mean cup depth. Table 4 also shows the

Table 1. Demographic and Clinical Characteristics of the Preperimetric Glaucoma and Control Study Groups

Characteristics	Glaucoma (n = 48)	Control (n = 86)	*P Value*
Age, yrs*	66.1±9.3	63.6±10.8	0.238
Gender, % male	50.0	32.6	0.097
Ancestry, % African-American	16.6	4.3	0.057
MD, dB†	–0.63±1.24	0.09±1.33	0.002
PSD, dB†	1.61 (1.43, 1.56, 1.77)	1.55 (1.28, 1.46, 1.70)	0.136
Disc area, mm^2*	1.97±0.08	1.97±0.06	0.927
Intraocular pressure, mmHg*	19.77±0.56	19.97±0.70	0.825
Signal strength of the Spectralis SD-OCT (Heidelberg Engineering, Carlsbad, CA) images*	23.95±0.53	23.58±0.42	0.582
Quality of the HRT-III (Heidelberg Engineering) images, SD†	18.31 (13, 18, 20.5)	17.31 (13, 15, 20)	0.212
Follow-up, yrs*	14.0±3.6	14.9±4.2	0.466
Ametropia, D*	–0.81±0.30	–0.70±0.27	0.795
Axial length, mm*	24.09±0.16	24.01±0.15	0.709
Average corneal curvature, mm*	7.72±0.04	7.78±0.03	0.274
Pachymetry, μm*	569.74±6.49	579.14±5.93	0.288

D = diopter; dB = decibels; HRT-III = Heidelberg Retinal Tomograph III; MD = mean deviation; PSD = pattern standard deviation; SD = standard deviation; SD-OCT = spectral domain optical coherence tomography.
*Normally distributed variables; represented by mean (SD).
†Non-normally distributed variables; represented by mean (first quartile, median, third quartile).

AUC for each parameter. The parameters with the largest AUCs were rim area (0.72±0.05), rim volume (0.71±0.05), and linear cup-to-disk ratio (0.66±0.05). The contour line-independent parameter global GPS had an AUC of 0.64 (±0.05). Figure 2 shows the ROC curves for rim area, rim volume, and global GPS of the CSLO.

Table 5 presents LRs with 95% CIs for the HRT-III MRA. Outside normal limits results were generally associated with small or insignificant effects on the post-test probability of disease, except for the temporal inferior sector that was associated with large effect (LR = 17.91). Borderline and within normal limits results were associated with insignificant to small effects. For the overall classification, both an outside normal limit result (LR = 3.19) and a within normal limit result (LR = 0.42) were associated with small changes in the probability of disease. A borderline result was associated with insignificant change in the probability of disease (LR = 0.82).

The SD-OCT parameter with the largest AUC, temporal superior RNFL thickness, performed significantly better than the CSLO parameter with the largest AUC, rim area (0.88 vs. 0.72; P=0.008), for differentiating between the preperimetric glaucoma and control groups. Table 6 shows the comparison of the diagnostic accuracy of SD-OCT RNFL thickness parameters with the best performing CSLO parameter (rim area), according to the sectors around the optic disc. Statistical comparison of AUCs between instruments showed significant differences between SD-OCT RNFL thickness and CSLO rim area for the temporal superior (0.88 vs 0.68; P=0.001) and temporal inferior (0.81 vs 0.64; P=0.01) sectors. Figure 3 shows ROC curves of the temporal superior average RNFL thickness measured by the SD-OCT and the temporal superior rim area measured by the CSLO.

Discussion

The present study demonstrated that RNFL assessment with Spectralis SD-OCT was able to detect preperimetric glaucomatous damage in eyes with suspected glaucoma. In addition, SD-OCT performed better than topographic optic

Table 2. Mean ± Standard Deviation Values of Spectral Domain Optical Coherence Tomography Retinal Nerve Fiber Layer Parameters with Area Under the Receiver Operating Characteristic Curves and Sensitivities at Fixed Specificities for Discriminating between Preperimetric Glaucoma and Control Groups

Parameter	Glaucoma (n = 48)	Control (n = 86)	*P Value**	AUC (SE)	Sensitivity (Specificity = 80%)	Sensitivity (Specificity = 95%)
Temporal superior thickness	102.0±3.3	128.8±2.0	<0.001	0.88 (0.03)	80.2%	47.6%
Global thickness	78.2±2.0	92.8±1.2	<0.001	0.86 (0.03)	73.2%	25.5%
Temporal inferior thickness	109.2±4.0	136.3±2.1	<0.001	0.81 (0.04)	53.4%	33.7%
Nasal superior thickness	79.3±3.6	93.0±2.2	<0.001	0.73 (0.05)	34.8%	15.1%
Nasal thickness	59.7±2.6	69.6±1.5	<0.001	0.70 (0.05)	38.3%	15.1%
Nasal inferior thickness	88.1±4.3	106.0±3.2	<0.001	0.68 (0.04)	37.2%	25.5%
Temporal thickness	63.2±2.8	69.0±1.5	0.04	0.62 (0.05)	27.9%	15.1%

AUC = area under the receiver operating characteristic curve; SE = standard error.
*For comparison of mean values of spectral domain optical coherence tomography parameters between preperimetric glaucomatous and control eyes.

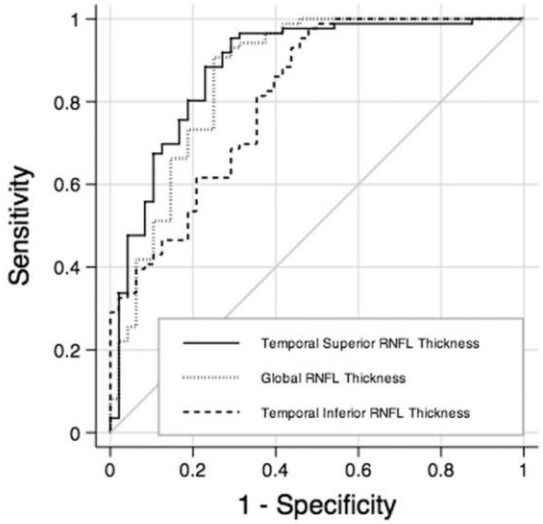

Figure 1. The receiver operating characteristic curves for temporal superior thickness, global thickness, and temporal inferior thickness obtained by spectral domain optical coherence tomography. RNFL = retinal nerve fiber layer.

disc assessment obtained with CSLO. These findings may have significant implications for the use of SD-OCT technology as an ancillary test in the diagnostic evaluation of glaucoma suspects.

Several studies have investigated the ability of SD-OCT to detect glaucomatous damage. In previous investigations, the diagnostic accuracy usually was assessed on the basis of the ability of the tested parameters to differentiate eyes with repeatable glaucomatous visual field loss from those of healthy subjects.[11,12,17–21] Such investigations are important to provide an initial assessment of the ability of the instrument to detect damage. In other words, if the instrument fails to separate these 2 clearly distinct groups, it would generally be regarded as not useful for diagnostic purposes. However, in clinical practice, a diagnostic test is used to diagnose disease in patients with suspected disease, not in patients with confirmed diagnosis. Therefore, if a test succeeds in initial diagnostic studies, further steps are needed to evaluate whether it is able to provide clinically relevant information. The evaluation of the ability of imaging devices to provide additional information to that of clinical examination and visual field testing is fundamental to measure their true value as complementary tests for diagnosing glaucoma in patients with suspicious findings for the disease. The design of our study enabled the evaluation of the performance of these tests in the clinically relevant situation of diagnosing disease in patients with suspicious appearance of the optic disc.

Our estimates of diagnostic accuracy were generally lower than those reported by studies investigating only patients with glaucomatous visual field loss.[3–9,11–13,16–21] Leung et al[19] compared SD-OCT and CSLO in discriminating eyes with glaucomatous visual field damage from those of healthy subjects and found an AUC of 0.978 for the SD-OCT parameter global RNFL thickness. In our study, we found a corresponding AUC of 0.86. A reasonable explanation for such different findings is that the accuracy of diagnostic instruments can vary according to the cohort investigated and the reference standard used to define disease.[36] The lower performance of the imaging instruments in our study compared with previous ones is probably related, at least in part, to the less severe stage of disease in patients with glaucoma included in our analyses. Because the patients did not have visual field damage at the time of imaging, they were likely at an earlier stage of disease than those included in previous studies using patients with visual field damage. Furthermore, the worse performance is also likely related to the method of selection of the control group. In our study, control subjects also had suspicious-appearing optic discs, making it more difficult for the diagnostic test to differentiate them from diseased subjects. Medeiros et al[25] evaluated the impact of design-related bias in studies of diagnostic tests in glaucoma and found that studies with a case-control design including patients with well-established disease and a separate group of normal (unsuspected) control subjects resulted in substantial overestimation of the performance of the tests.

We used evidence of previously documented progressive optic disc change as the reference standard to classify glaucoma suspects as disease positive versus disease negative. In the absence of visual field loss, glaucoma can be diag-

Table 3. Likelihood Ratios and 95% Confidence Intervals for Spectral Domain Optical Coherence Tomography Parameters

Parameter	Within Normal Limits	Borderline	Outside Normal Limits
Temporal superior thickness	0.44 (0.12–0.77)	21.50 (19.49–23.50)	26.87 (24.88–28.86)
Global thickness	0.39 (0.02–0.76)	5.37 (4.29–6.45)	Infinity (NA)
Temporal inferior thickness	0.48 (0.18–0.78)	21.50 (19.49–23.50)	Infinity (NA)
Nasal superior thickness	0.71 (0.50–0.92)	4.30 (3.31–5.28)	7.16 (5.00–9.32)
Nasal thickness	0.89 (0.78–1.00)	4.47 (2.87–6.08)	Infinity (NA)
Nasal inferior thickness	0.92 (0.83–1.01)	0.92 (0.83–1.01)	Infinity (NA)
Temporal thickness	0.82 (0.66–0.99)	2.09 (1.05–3.12)	Infinity (NA)
Overall classification	0.26 (0–0.82)	1.05 (0.35–1.75)	50.16 (48.20–52.12)

NA = not applicable.

Table 4. Mean ± Standard Deviation Values of Confocal Scanning Laser Ophthalmoscopy Parameters with Areas Under the Receiver Operating Characteristic Curves and Sensitivities at Fixed Specificities for Discriminating between Preperimetric Glaucoma and Control Groups

Parameter	Glaucoma (n = 48)	Control (n = 86)	*P Value**	AUC (SE)	Sensitivity (Specificity = 80%)	Sensitivity (Specificity = 95%)
Rim area (mm^2)	1.20±0.05	1.38±0.03	<0.001	0.72 (0.05)	41.8%	10.4%
Rim volume (mm^3)	0.30±0.02	0.38±0.01	0.002	0.71 (0.05)	52.3%	11.6%
Linear cup-to-disk ratio	0.59±0.02	0.52±0.01	0.002	0.66 (0.05)	41.6%	25.0%
Cup-to-disk area ratio	0.36±0.02	0.28±0.01	0.003	0.66 (0.05)	41.6%	22.9%
Rim-to-disk area ratio	0.63±0.02	0.71±0.01	0.003	0.66 (0.05)	29.0%	6.9%
RNFL CSA (mm^2)	1.07±0.07	1.29±0.05	0.005	0.65 (0.05)	38.3%	17.4%
Global GPS	0.54±0.05	0.38±0.03	0.006	0.64 (0.05)	45.8%	16.6%
Mean RNFL thickness (mm)	0.22±0.01	0.26±0.01	0.004	0.64 (0.05)	36.0%	9.3%
Cup area (mm^2)	0.78±0.08	0.59±0.04	0.023	0.62 (0.06)	37.5%	18.7%
Cup volume (mm^3)	0.24±0.04	0.14±0.01	0.016	0.62 (0.05)	35.4%	16.6%
Mean cup depth (mm)	0.28±0.02	0.25±0.01	0.071	0.58 (0.06)	33.3%	10.4%

AUC = area under the receiver operating characteristic curve; CSA = cross-sectional area; GPS = glaucoma probability score; RNFL = retinal nerve fiber layer; SE = standard error.
*For comparison of mean values of confocal scanning laser ophthalmoscopy parameters between glaucomatous and control eyes.

nosed with certainty only by demonstrating a history of progressive glaucomatous changes to the optic nerve. This approach was first proposed by Medeiros et al[24] for evaluation of diagnostic tests in glaucoma. The presence of progressive optic disc damage is also highly predictive of future development of visual field defects.[37] However, although it enables the evaluation of diagnostic accuracy in a situation that better resembles clinical practice, it still has some limitations. It is possible, for example, that some patients who had glaucomatous optic disc damage were not included because they did not present with progressive damage during the follow-up period. Patients with suspicious optic disc appearance who did not show any evidence of optic disc change or visual field loss during follow-up were considered as controls. It might be argued that some of these patients from the control group could have had glaucomatous damage to the optic disc or might develop visual field defects, but the follow-up time was insufficient to detect progression. Although it is unlikely that patients with glaucoma would not progress or develop functional loss followed untreated for an average of 14 years, this possibility cannot be completely excluded. Another limitation of this study design is that stereophotographic evaluation of optic disc change has an imperfect interobserver agreement.[38] As a consequence, some eyes could be misdiagnosed and incorrectly designated to the glaucomatous or the control group. However, to minimize misclassifications, we required consensus grading by 2 trained expert ophthalmologists, and a third experienced grader reviewed the stereophotographs in cases of disagreement.

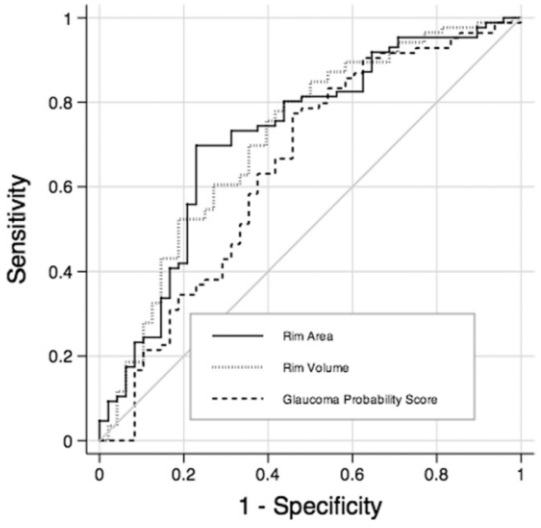

Figure 2. The receiver operating characteristic curves for rim volume, rim area, and glaucoma probability score parameters obtained by confocal scanning laser ophthalmoscopy.

In the present study, the Spectralis SD-OCT parameters with highest diagnostic accuracies were the temporal superior, global, and temporal inferior RNFL thickness measurements, with AUCs of 0.88, 0.86, and 0.81, respectively. RNFL losses in the temporal superior and temporal inferior sectors are expected and correspond to initial stages of optic nerve damage in patients with glaucoma.[12,18,39] The poor performance of the temporal and nasal sectors can be justified by the fact that those sectors are more frequently affected in advanced glaucoma, and our population is composed mostly of individuals with early damage. The RNFL parameters performed significantly better than topographic parameters in differentiating glaucomatous and control eyes. Temporal superior average RNFL thickness was the parameter with the best performance for the Spectralis SD-OCT, with an AUC of 0.88, whereas rim area was the parameter with the best performance for the CSLO, with an AUC of 0.72. Given the selection criteria of our study, these results are not surprising and are similar to those found in a previous study comparing RNFL assessment by scanning laser polarimetry with CSLO.[22] The difference in ancestry

Table 5. Likelihood Ratios and 95% Confidence Intervals for Confocal Scanning Laser Ophthalmoscopy Moorfields Regression Analysis

Parameter	Within Normal Limits	Borderline	Outside Normal Limits
Temporal superior	0.71 (0.46–0.95)	2.50 (1.77–3.23)	2.98 (1.59–4.37)
Global	0.59 (0.29–0.89)	2.32 (1.58–3.07)	4.92 (3.83–6.01)
Temporal inferior	0.50 (0.17–0.84)	2.76 (2.09–3.44)	17.91 (15.89–19.94)
Nasal superior	0.66 (0.39–0.92)	2.86 (1.80–3.92)	3.32 (2.47–4.17)
Nasal	0.77 (0.53–1.02)	0.89 (0–1.90)	3.32 (2.47–4.17)
Nasal inferior	0.61 (0.28–0.94)	1.15 (0.39–1.91)	3.80 (3.04–4.56)
Temporal	0.86 (0.70–1.01)	2.55 (1.66–3.45)	1.79 (0–4.54)
Overall classification	0.42 (0–0.98)	0.82 (0.24–1.41)	3.19 (2.64–3.75)

between groups was marginally significant in our study. Although previous studies reported that ancestry did not influence the diagnostic performance of the SD-OCT technology,[40] we performed an additional analysis excluding black patients. As expected, similar results were achieved, with SD-OCT temporal superior RNFL thickness performing better than CSLO rim area (0.87 vs. 0.73; $P=0.031$).

The starting point of a diagnostic process occurs when a clinician combines the medical history with clinical examination to estimate the probability of the presence of the disease, also known as pretest probability. The results of diagnostic tests are then used to modify the pretest probability of disease, yielding a new post-test probability. The direction and magnitude of this change from pretest to post-test are determined by the test's properties, in particular by the LR of the test. The LR represents the magnitude of change from a clinician's initial suspicion for disease (pretest probability) to the likelihood of disease after the test result (post-test probability). In our study, outside normal limits results for Spectralis SD-OCT parameters were generally associated with large changes from the pretest to post-test probability of disease. In contrast, outside normal limits results for the HRT-III MRA were only associated with insignificant to small effects. This means that an abnormal result on Spectralis SD-OCT would have a larger impact in increasing the probability of disease than an abnormal result found on the MRA provided by the CSLO. For within normal limits, the LR for the overall Spectralis SD-OCT classification was smaller (i.e., better) than the overall classification for MRA (0.26 vs 0.42), indicating that normal results on SD-OCT would carry more impact in excluding the disease than those from CSLO. The evaluation of the integrity of the RNFL during clinical examination is difficult, especially in older patients with light pigmented retinas or hazy optical media. However, evaluation of the optic nerve and identification of areas of suspicious rim thinning or optic disc cupping are more straightforward. Therefore, patients with suspicious disc appearance will generally be those with large cups or suspicious rim thinning. In these patients, it is not surprising that topographic information about cup size or cup depth, for example, does not provide much additional information in terms of establishing the definitive diagnosis.

The design of our study evaluates a diagnostic test in a scenario that resembles the use of imaging devices in clinical practice for assisting in detecting damage in glaucoma suspects. However, this design might not be the most appropriate for other situations, such as when assessing the ability of an instrument to screen for patients with glaucomatous visual field loss in the general population. There-

Table 6. Areas Under the Receiver Operating Characteristic Curves ± Standard Error of Spectral Domain Optical Coherence Tomography Retinal Nerve Fiber Layer Parameters and Confocal Scanning Laser Ophthalmoscopy Rim Area by Sectors

Sector	SD-OCT	CSLO	*P Value*
Temporal superior	0.88±0.03	0.68±0.05	0.001
Temporal inferior	0.81±0.04	0.64±0.05	0.01
Nasal superior	0.73±0.05	0.67±0.05	0.40
Nasal	0.70±0.05	0.66±0.05	0.52
Nasal inferior	0.68±0.04	0.61±0.05	0.27
Temporal	0.62±0.05	0.60±0.05	0.75

CSLO = confocal scanning laser ophthalmoscopy; SD-OCT = spectral domain optical coherence tomography.

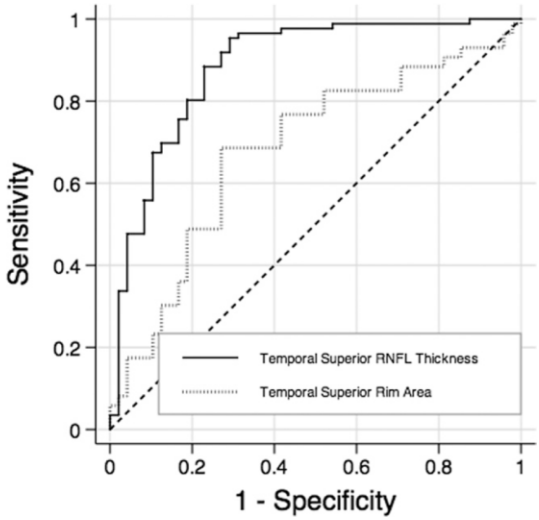

Figure 3. The receiver operating characteristic curves for temporal superior thickness obtained by spectral-domain optical coherence tomography and temporal superior rim area obtained by confocal scanning laser ophthalmoscopy. RNFL = retinal nerve fiber layer.

fore, the study design should take into account the context and clinical situation in which the diagnostic test will be applied. In addition, it should be noted that longitudinal follow-up of glaucoma suspects and patients with glaucoma may represent the most advantageous use of these technologies in clinical practice.[23,24] In fact, in many glaucoma suspects, confirmation about the presence or absence of disease will be possible only after careful long-term follow-up, and imaging devices could be used to monitor structural changes in this situation.

In conclusion, our results showed that RNFL imaging with Spectralis SD-OCT performed well in detecting preperimetric glaucomatous damage in glaucoma suspects, presenting a better diagnostic capability than topographic assessment with the CSLO. Abnormal results on SD-OCT (compared with the instrument's normative database) were associated with high LRs and large effects on post-test probabilities of having preperimetric glaucomatous damage.

References

1. Nassif N, Cense B, Park B, et al. In vivo high-resolution video-rate spectral-domain optical coherence tomography of the human retina and optic nerve. Opt Express [serial online] 2004;12:367–76. Available at: http://www.opticsinfobase.org/oe/abstract.cfm?uri=oe-12-3-367. Accessed May 21, 2012.
2. Wojtkowski M, Srinivasan V, Ko T, et al. Ultrahigh-resolution, high-speed, Fourier domain optical coherence tomography and methods for dispersion compensation. Opt Express [serial online] 2004;12:2404–22. Available at: http://www.opticsinfobase.org/oe/abstract.cfm?uri=oe-12-11-2404. Accessed May 21, 2012.
3. Mistlberger A, Liebmann JM, Greenfield DS, et al. Heidelberg retina tomography and optical coherence tomography in normal, ocular-hypertensive, and glaucomatous eyes. Ophthalmology 1999;106:2027–32.
4. Zangwill LM, Bowd C, Berry CC, et al. Discriminating between normal and glaucomatous eyes using the Heidelberg Retina Tomograph, GDx Nerve Fiber Analyzer, and Optical Coherence Tomograph. Arch Ophthalmol 2001;119:985–93.
5. Greaney MJ, Hoffman DC, Garway-Heath DF, et al. Comparison of optic nerve imaging methods to distinguish normal eyes from those with glaucoma. Invest Ophthalmol Vis Sci 2002;43:140–5.
6. Medeiros FA, Zangwill LM, Bowd C, Weinreb RN. Comparison of the GDx VCC scanning laser polarimeter, HRT II confocal scanning laser ophthalmoscope, and Stratus OCT optical coherence tomograph for the detection of glaucoma. Arch Ophthalmol 2004;122:827–37.
7. Jindal S, Dada T, Sreenivas V, et al. Comparison of the diagnostic ability of Moorfield's regression analysis and glaucoma probability score using Heidelberg retinal tomograph III in eyes with primary open angle glaucoma. Indian J Ophthalmol 2010;58:487–92.
8. Rao HL, Babu GJ, Sekhar GC. Comparison of the diagnostic capability of the Heidelberg retina tomographs 2 and 3 for glaucoma in the Indian population. Ophthalmology 2010;117:275–81.
9. Naithani P, Sihota R, Sony P, et al. Evaluation of optical coherence tomography and Heidelberg retinal tomography parameters in detecting early and moderate glaucoma. Invest Ophthalmol Vis Sci 2007;48:3138–45.
10. Medeiros FA, Zangwill LM, Bowd C, et al. Evaluation of retinal nerve fiber layer, optic nerve head, and macular thickness measurements for glaucoma detection using optical coherence tomography. Am J Ophthalmol 2005;139:44–55.
11. Wang X, Li S, Fu J, et al. Comparative study of retinal nerve fibre layer measurement by RTVue OCT and GDx VCC. Br J Ophthalmol 2011;95:509–13.
12. Park SB, Sung KR, Kang SY, et al. Comparison of glaucoma diagnostic capabilities of Cirrus HD and Stratus optical coherence tomography. Arch Ophthalmol 2009;127:1603–9.
13. Chang RT, Knight OJ, Feuer WJ, Budenz DL. Sensitivity and specificity of time-domain versus spectral-domain optical coherence tomography in diagnosing early to moderate glaucoma. Ophthalmology 2009;116:2294–9.
14. Parikh RS, Parikh S, Sekhar GC, et al. Diagnostic capability of optical coherence tomography (Stratus OCT 3) in early glaucoma. Ophthalmology 2007;114:2238–43.
15. Hougaard JL, Heijl A, Bengtsson B. Glaucoma detection by Stratus OCT. J Glaucoma 2007;16:302–6.
16. Leung CK, Cheung CY, Weinreb RN, et al. Retinal nerve fiber layer imaging with spectral-domain optical coherence tomography: a variability and diagnostic performance study. Ophthalmology 2009;116:1257–63.
17. Rao HL, Zangwill LM, Weinreb RN, et al. Comparison of different spectral domain optical coherence tomography scanning areas for glaucoma diagnosis. Ophthalmology 2010;117:1692–9.
18. Sehi M, Grewal DS, Sheets CW, Greenfield DS. Diagnostic ability of Fourier-domain vs time-domain optical coherence tomography for glaucoma detection. Am J Ophthalmol 2009;148:597–605.
19. Leung CK, Ye C, Weinreb RN, et al. Retinal nerve fiber layer imaging with spectral-domain optical coherence tomography: a study on diagnostic agreement with Heidelberg Retinal Tomograph. Ophthalmology 2010;117:267–74.
20. Leung CK, Lam S, Weinreb RN, et al. Retinal nerve fiber layer imaging with spectral-domain optical coherence tomography: analysis of the retinal nerve fiber layer map for glaucoma detection. Ophthalmology 2010;117:1684–91.
21. Leite MT, Rao HL, Zangwill LM, et al. Comparison of the diagnostic accuracies of the Spectralis, Cirrus, and RTVue optical coherence tomography devices in glaucoma. Ophthalmology 2011;118:1334–9.
22. Medeiros FA, Vizzeri G, Zangwill LM, et al. Comparison of retinal nerve fiber layer and optic disc imaging for diagnosing glaucoma in patients suspected of having the disease. Ophthalmology 2008;115:1340–6.
23. Medeiros FA. How should diagnostic tests be evaluated in glaucoma? Br J Ophthalmol 2007;91:273–4.
24. Medeiros FA, Zangwill LM, Bowd C, et al. Use of progressive glaucomatous optic disk change as the reference standard for evaluation of diagnostic tests in glaucoma. Am J Ophthalmol 2005;139:1010–8.
25. Medeiros FA, Ng D, Zangwill LM, et al. The effects of study design and spectrum bias on the evaluation of diagnostic accuracy of confocal scanning laser ophthalmoscopy in glaucoma. Invest Ophthalmol Vis Sci 2007;48:214–22.
26. Leite MT, Rao HL, Weinreb RN, et al. Agreement among spectral-domain optical coherence tomography instruments for assessing retinal nerve fiber layer thickness. Am J Ophthalmol 2011;151:85–92.
27. Swindale NV, Stjepanovic G, Chin A, Mikelberg FS. Automated analysis of normal and glaucomatous optic nerve head topography images. Invest Ophthalmol Vis Sci 2000;41:1730–42.
28. Wollstein G, Garway-Heath DF, Hitchings RA. Identification of early glaucoma cases with the scanning laser ophthalmoscope. Ophthalmology 1998;105:1557–63.

29. Dodd LE, Pepe MS. Partial AUC estimation and regression. Biometrics 2003;59:614–23.
30. Zhou XH, Obuchowski NA, McClish DK. Analysis of correlated ROC data. In: Zhou XH, Obuchowski NA, McClish DK, eds. Statistical Methods in Diagnostic Medicine. New York: Wiley; 2002:274–306.
31. Alonzo TA, Pepe MS. Distribution-free ROC analysis using binary regression techniques. Biostatistics 2002;3:421–32.
32. Radack KL, Rouan G, Hedges J. The likelihood ratio: an improved measure for reporting and evaluating diagnostic test results. Arch Pathol Lab Med 1986;110:689–93.
33. Jaeschke R, Guyatt GH, Sackett DL; Evidence-Based Medicine Working Group. Users' guides to the medical literature. III. How to use an article about a diagnostic test. B. What are the results and will they help me in caring for my patients? JAMA 1994;271:703–7.
34. Fagan TJ. Letter: Nomogram for Bayes theorem. N Engl J Med 1975;293:257.
35. Simel DL, Samsa GP, Matchar DB. Likelihood ratios with confidence: sample size estimation for diagnostic test studies. J Clin Epidemiol 1991;44:763–70.
36. Lijmer JG, Mol BW, Heisterkamp S, et al. Empirical evidence of design-related bias in studies of diagnostic tests. JAMA 1999;282:1061–6.
37. Medeiros FA, Alencar LM, Zangwill LM, et al. Prediction of functional loss in glaucoma from progressive optic disc damage. Arch Ophthalmol 2009;127:1250–6.
38. Breusegem C, Fieuws S, Stalmans I, Zeyen T. Agreement and accuracy of non-expert ophthalmologists in assessing glaucomatous changes in serial stereo optic disc photographs. Ophthalmology 2011;118:742–6.
39. Moreno-Montanes J, Olmo N, Alvarez A, et al. Cirrus high-definition optical coherence tomography compared with Stratus optical coherence tomography in glaucoma diagnosis. Invest Ophthalmol Vis Sci 2010;51:335–43.
40. Girkin CA, Liebmann J, Fingeret M, et al. The effects of race, optic disc area, age, and disease severity on the diagnostic performance of spectral-domain optical coherence tomography. Invest Ophthalmol Vis Sci 2011;52:6148–53.

Footnotes and Financial Disclosures

Originally received: February 15, 2012.
Final revision: April 11, 2012.
Accepted: June 4, 2012.
Available online: August 9, 2012. Manuscript no. 2012-229.

[1] Hamilton Glaucoma Center, Department of Ophthalmology, University of California San Diego, La Jolla, California.

[2] Federal University of São Paulo, Department of Ophthalmology, São Paulo, Brazil.

Financial Disclosure(s):
The author(s) have made the following disclosure(s):
L.M.Z.- financial support from Carl Zeiss Meditec Inc. and Heidelberg Engineering; A.T.- none; R.N.W.: Financial support from Alcon, Allergan, Merck, Bausch & Lomb, Zeiss Meditec, Optovue, Novartis, Nidek, Topcon, and Aeries; F.A.M.: financial support from Carl-Zeiss Meditec, Inc. and Heidelberg Engineering, GmBH.

Supported in part by National Institutes of Health/National Eye Institute Grants EY021818 (F.A.M.), EY11008 (L.M.Z.), and EY14267 (L.M.Z.), CAPES grand BEX 1066/11-0, an unrestricted grant from Research to Prevent Blindness (New York, NY), and a grant for participants' glaucoma medications from Alcon, Allergan, Pfizer, Merck, and Santen.

Correspondence: Felipe A. Medeiros, MD, Department of Ophthalmology, University of California, 9415 Campus Point Drive, La Jolla, CA 92037-0946. E-mail: fmedeiros@glaucoma.ucsd.edu.

2.2. Comparison of Different Specral Domain OCT Scanning Protocols for Diagnosing Preperimetric Glaucoma

Renato Lisboa, MD; Augusto Paranhos Jr, MD, PhD; Robert N. Weinreb, MD; Linda M. Zangwill, PhD; Mauro T. Leite, MD, PhD ; Felipe A. Medeiros, MD, PhD.

Investigative Ophthalmology & Visual Science, 2013 Mar; 54(5):3417-25

Glaucoma

Comparison of Different Spectral Domain OCT Scanning Protocols for Diagnosing Preperimetric Glaucoma

Renato Lisboa,[1,2] Augusto Paranhos Jr,[2] Robert N. Weinreb,[1] Linda M. Zangwill,[1] Mauro T. Leite,[2] and Felipe A. Medeiros[1]

[1]Hamilton Glaucoma Center, Department of Ophthalmology, University of California-San Diego, La Jolla, California
[2]Department of Ophthalmology, Federal University of São Paulo, São Paulo, Brazil

Correspondence: Felipe A. Medeiros, Hamilton Glaucoma Center, University of California-San Diego, 9500 Gilman Drive, La Jolla, CA 92093; fmedeiros@glaucoma.ucsd.edu.

Submitted: January 17, 2013
Accepted: March 12, 2013

Citation: Lisboa R, Paranhos A Jr, Weinreb RN, Zangwill LM, Leite MT, Medeiros FA. Comparison of different spectral domain OCT scanning protocols for diagnosing preperimetric glaucoma. *Invest Ophthalmol Vis Sci*. 2013;54:3417–3425. DOI:10.1167/iovs.13-11676

Purpose. To compare the ability of spectral-domain optical coherence tomography (SDOCT) retinal nerve fiber layer (RNFL), optic nerve head (ONH), and macular measurements to detect preperimetric glaucomatous damage.

Methods. The study included 142 eyes from 91 patients suspected of having the disease based on the appearance of the optic disc. All eyes had normal visual fields before the imaging session. Forty-eight eyes with progressive glaucomatous damage were included in the preperimetric glaucoma group. Ninety-four eyes without any evidence of progressive glaucomatous damage and followed untreated for 12.8 ± 3.6 years were used as controls. Areas under the receiver operating characteristic curves (AUC) were calculated to summarize diagnostic accuracies of the parameters.

Results. The three RNFL parameters with the largest AUCs were average RNFL thickness (0.89 ± 0.03), inferior hemisphere average thickness (0.87 ± 0.03), and inferior quadrant average thickness (0.85 ± 0.03). The three ONH parameters with the largest AUCs were vertical cup-to-disc ratio (0.74 ± 0.04), rim area (0.72 ± 0.05), and rim volume (0.72 ± 0.05). The three macular parameters with the largest AUCs were GCC average thickness (0.79 ± 0.04), GCC inferior thickness (0.79 ± 0.05), and GCC superior thickness (0.76 ± 0.05). Average RNFL thickness performed better than vertical cup-to-disc ratio (0.89 vs. 0.74; $P = 0.007$) and GCC average thickness (0.89 vs. 0.79; $P = 0.015$).

Conclusions. SDOCT RNFL measurements performed better than ONH and macular measurements for detecting preperimetric glaucomatous damage in a cohort of glaucoma suspects. (ClinicalTrials.gov number, NCT00221897.)

Keywords: preperimetric, glaucoma, diagnosis

Structural assessment of the optic nerve is an essential component of glaucoma diagnosis and management.[1–4] The use of spectral-domain optical coherence tomography (SDOCT) technology has enabled clinicians to obtain unprecedented high-resolution images of the optic nerve head (ONH) and retinal nerve fiber layer (RNFL) structures in a fraction of the time required by previous technologies. SDOCT is also able to image the macular area, where the highest concentration of ganglion cells is found, and macular imaging has been proposed as a useful tool for structural assessment of glaucomatous damage.[5]

Several previous studies have evaluated the accuracies of RNFL, ONH, and macula scans provided by SDOCT for glaucoma diagnosis.[6–10] Although these studies are important in providing an initial assessment and comparison of these scanning areas, their estimates of diagnostic accuracy might not directly correspond to the performance of these tests when used in clinical practice. In these studies, diagnostic accuracy was assessed based on the ability to differentiate patients with clearly defined glaucomatous visual field damage from healthy eyes without any suspicious findings for the disease. However, in clinical practice, one is interested in the ability of the diagnostic test in evaluating the presence of disease in those suspected of a condition, not in those with clearly defined diagnoses. Therefore, to justify the cost and expense of applying an additional diagnostic test for glaucoma evaluation, it is important to demonstrate its benefit in providing additional clinical information besides what can be gathered from the conventional clinical examination and visual field assessment. In the absence of clearly defined visual field losses, SDOCT could potentially be used to differentiate eyes with preperimetric glaucomatous damage from eyes that show suspicious optic disc appearances, but no structural damage.

The purpose of this study was to evaluate and compare the accuracies of SDOCT assessment of RNFL, ONH, and macular areas for diagnosing preperimetric glaucoma in a cohort of patients suspected of having the disease. Documented longitudinal assessment of the optic nerve was used as the reference standard to establish the final diagnosis of preperimetric damage and allow comparison of the accuracies of the different scanning areas.[11–15]

Methods

Participants

This was an observational cohort study that included patients recruited from the Diagnostic Innovations in Glaucoma Study (DIGS) conducted at the Hamilton Glaucoma Center (University

Investigative Ophthalmology & Visual Science

of California-San Diego). Participants were longitudinally evaluated according to an established protocol that included visits with complete clinical examination and several imaging and functional tests. All participants who met the inclusion criteria described below were enrolled and all data were entered in a computer database. Informed consent was obtained from all participants. The University of California-San Diego Human Subjects Committee approved all protocols, and methods described adhered to the tenets of the Declaration of Helsinki.

Each subject underwent a comprehensive ophthalmic examination, including review of medical history, best corrected visual acuity, slit-lamp biomicroscopy, IOP measurement using Goldmann applanation tonometry, gonioscopy, dilated fundoscopic examination using a 78-diopter (D) lens, stereoscopic optic disc photography, and standard automated perimetry (SAP) with 24-2 Swedish Interactive Threshold Algorithm (Carl Zeiss Meditec, Inc., Dublin, CA).

To be included, subjects had to have best-corrected visual acuity of 20/40 or better, spherical refraction within ±5.0 D, cylinder correction within 3.0 D, and open angle with gonioscopy. Subjects with coexisting retinal disease, uveitis, or nonglaucomatous optic disc neuropathy were excluded from the study.

A cohort of participants suspected of having glaucoma was selected from our database. These participants were initially selected based on the presence of suspicious appearance of the optic nerve from cross-sectional evaluation of stereophotographs at the time of imaging by two independent masked graders. A third grader reviewed the stereophotographs in case of disagreement. Features characteristic of suspicious glaucomatous appearance of the optic disc were neuroretinal rim narrowing, cupping, or suspicious RNFL defects. All participants had a normal SAP visual field result at the time of imaging. A normal visual field was defined as a mean deviation and pattern standard deviation within 95% confidence limits and a glaucoma hemifield test result within normal limits. Additionally, participants did not have repeatable glaucomatous visual field loss before the date of their examination with imaging instruments. All participants had been previously followed for at least 5 years before their imaging session.

These participants were then classified into cases and controls based on history of documented evidence of progressive glaucomatous change in the appearance of the optic disc occurring *before* the imaging sessions. Patients with documented evidence of progressive glaucomatous nerve damage at any time before both imaging sessions with SDOCT were considered as having preperimetric glaucoma. That is, preperimetric glaucoma was defined based on the presence of documented evidence of progressive structural damage to the optic nerve in the absence of visual field loss on SAP. Progressive glaucomatous change in the appearance of the optic disc was assessed by simultaneous stereophotographs (TRC-SS; Topcon Instrument Corp. of America, Paramus, NJ). Stereophotographic sets of slides were examined using a stereoscopic viewer (Asahi; Pentax, Tokyo, Japan). The stereophotographs were evaluated by two experienced graders, and each was masked to the subject's identity, to other test results, and to the chronological sequence of the stereophotographs. For inclusion, stereophotographs needed to be graded adequate or better. Definition of change was based on focal or diffuse narrowing of the neuroretinal rim, increased excavation, or enlargement of the RNFL defects. Changes on rim color, presence of disc hemorrhages, or progressive peripapillary atrophy were not sufficient for characterization of progression. Discrepancies between the two graders were resolved by either consensus or adjudication of a third experienced grader.

A total of 48 eyes from 42 participants with progressive optic disc damage and no visual field loss were included in the preperimetric glaucoma group. These subjects were followed for an average of 13.6 ± 4.2 years.

Patients without any evidence of progressive change in the appearance of the optic disc and without any evidence of visual field loss in both eyes were used as controls. Control eyes were also required to have no history of treatment during follow-up in order to avoid a confounding effect of treatment in preventing the development of progressive disc damage. A total of 94 eyes from 49 patients were included as a control group. These subjects had been followed untreated for an average of 12.8 ± 3.6 years without showing any evidence of progressive damage to the optic nerve.

Instrumentation

RTVue (software version 6.1.0.4; Optovue, Inc., Fremont, CA) was used to obtain SDOCT scans. RTVue uses a superluminescent diode scan with a center wavelength of 840 nm to provide high-resolution images. The instrument is able to collect 26,000 A-scans per second with an axial resolution of 5 μm. The ONH protocol and ganglion cell complex (GCC) protocol were used in this study. All patients had both protocols performed within 6 months of each other.

Peripapillary Retinal Nerve Fiber Layer Measurements. The ONH protocol was used to obtain RNFL measurements. This protocol generates an RNFL thickness map measured along a circle of 3.45 mm in diameter centered at the ONH. After the RNFL map is obtained, the RNFL thickness parameters are estimated by assessing a total of 2325 data points between the anterior and posterior RNFL borders. Several subdivisions of the entire measurement circle are performed. First, the overall average, together with the superior hemisphere, inferior hemisphere, temporal quadrant, superior quadrant, nasal quadrant, and inferior quadrant are provided. Then, each quadrant is divided in two, generating eight sectors of 45°. Finally, each 45° sector is divided into two more sectors, generating 16 sectors of 22.5°. Only good-quality images, as defined by a signal strength index greater than or equal to 28, were included in the analyses.

Optic Nerve Head Measurements. The ONH protocol was used to obtain ONH measurements. It consists of 12 radial scans of 3.4 mm in length (455 A-scans each) and 13 concentric circular scans ranging from 1.3 to 4.9 mm in diameter (425–965 A-scans each) and centered at the ONH. This protocol provides 14,141 A-scans in 0.55 seconds. Areas between the scans are interpolated. All images were processed with three-dimensional/video baseline. Although the delineation of the optic disc margin is automated, all images were reviewed. When necessary, images were manually delineated and centered at the optic disc by identifying and joining the RPE tips. The RTVue software (software version 6.1.0.4; Optovue, Inc.) automatically defines the optic cup as the intersection of the nerve head inner boundary and a parallel line that is 150 μm above the connecting line of the RPE tips. The ONH parameters measured by the software were rim area, rim volume, vertical cup-to-disc ratio, horizontal cup-to-disc ratio, cup area, cup volume, cup-to-disc area ratio, disc area, and nerve head volume. Only good-quality images, as defined by a signal strength index greater than or equal to 28, were included in the analyses.

Macular Measurements. The GCC protocol was used to obtain macular measurements. This protocol consists of one horizontal line scan of 7 mm in length (467 A-scans) followed by 15 vertical line scans of 7 mm in length (400 A-scans each) at 0.55-mm intervals. This protocol provides 14,810 A-scans in 0.58 seconds of a rectangular area. However, the area analyzed

by the software (RTVue, software version 6.1.0.4; Optovue, Inc.) involves a 6-mm-diameter circle inside the rectangular area scanned by the instrument. The analyzed circular area is centered 1 mm temporal to the fovea. This slight offset provides a more temporal retina analysis, which corresponds to the nasal visual field where glaucomatous damage is most likely to occur at initial stages of the disease (e.g., nasal step). The GCC protocol provides a segmentation of macular B-scans in two layers: GCC layer and outer retinal layer. The GCC layer is composed of the ganglion cell layer, the nerve fiber layer, and the inner plexiform layer. The GCC layer parameters generated by the GCC protocol are average thickness, superior thickness, inferior thickness, superior minus inferior thickness, global loss volume (GLV), focal loss volume (FLV), and root mean square (RMS). The calculations for GLV, FLV, and RMS have been described in detail elsewhere.[6] Briefly, GLV measures the average amount of GCC loss over the entire GCC map, whereas FLV measures the average amount of focal GCC loss over the entire GCC map. GLV best detects diffuse ganglion cell loss, similar to mean deviation in visual fields. Likewise, FLV best detects local ganglion cell loss using a pattern deviation map to correct for overall absolute changes, similar to pattern standard deviation in visual fields. The RMS or pattern coefficient of variation provides a summary of how well the fractional map (used to calculate the GLV) and pattern deviation map (used to calculate the FLV) of an individual fit the normal pattern. The worse the fit, the greater the value.

In addition to GCC layer parameters, the GCC protocol also evaluates the full retina and outer retina, separately. The parameters provided for each of them are average thickness, superior thickness, inferior thickness, and superior minus inferior thickness.

Only images acquired within 6 months of the ONH protocol and with good quality, as defined by a signal strength index greater than or equal to 32, were included in the analyses.

Statistical Analysis

Descriptive statistics included mean and SD for normally distributed variables and mean, first quartile, median, and third quartile for non-normally distributed variables.

To evaluate the ability of the parameters to differentiate between controls and preperimetric glaucomatous eyes, areas under the receiver operating characteristic (ROC) curves (AUC) were calculated. An AUC equal to 1 represents perfect discrimination, whereas an AUC of 0.5 represents chance discrimination. Sensitivity at fixed specificities of 80% and 95% were also reported for each parameter. AUCs were adjusted for sex differences between groups using the covariate adjusting procedure proposed by Pepe et al.[16] Pairwise comparisons of the AUCs were performed between the best parameters of each protocol.[16] A bootstrap resampling procedure ($n = 1000$ resamples) was used to derive the confidence intervals.[17] To account for potential correlation between eyes, the cluster of the data for the study subject was considered as the unit of resampling when calculating SEs. This procedure has been used to adjust for the presence of multiple correlated measurements of the same unit.[17,18]

All statistical analyses were performed with commercially available software (Stata version 11; Stata Corp., College Station, TX). The alpha level (type I error) was set at 0.05.

Results

Table 1 shows demographic and clinical characteristics of the eyes included in the study. No differences in age and ancestry were found between groups. There were more male subjects in the preperimetric glaucoma group than in the control group. Therefore, all ROC curves and comparisons were adjusted for sex differences between groups. Forty eyes included in the preperimetric group presented rim changes, whereas eight eyes presented changes on both RNFL and rim.

Peripapillary Retinal Nerve Fiber Layer Measurements

Table 2 shows mean values of RNFL parameters in the preperimetric glaucoma and control groups. Preperimetric glaucomatous eyes had, on average, significantly thinner RNFL measurements than control eyes. The three RNFL parameters with largest AUCs were average thickness (0.89 ± 0.03), inferior hemisphere average RNFL thickness (0.87 ± 0.03), and inferior quadrant RNFL thickness (0.85 ± 0.03). Pairwise comparisons did not demonstrate statistically significant differences between the AUCs of these parameters ($P > 0.05$ for all comparisons). The parameter with the highest sensitivity at fixed specificity of 95% was average thickness (70.8%). Figure 1 shows the ROC curves of the three RNFL parameters with largest AUCs.

Optic Nerve Head Measurements

Table 3 shows mean values of ONH parameters in the preperimetric glaucoma and control groups. Statistically significant differences were found for all parameters, except for disc area. The 3 ONH parameters with largest AUCs were vertical cup-to-disc ratio (0.74 ± 0.04), rim area (0.72 ± 0.05), and rim volume (0.72 ± 0.05). Pairwise comparisons did not show statistically significant differences between AUCs of these parameters ($P > 0.05$ for all comparisons). Rim area, rim volume, nerve head volume, and cup-to-disc area ratio showed the same sensitivity of 27.1% at fixed specificity of 95%. Figure 2 shows the ROC curves for the three ONH parameters with largest AUCs.

Macular Measurements

Table 4 shows mean values of macular parameters in the preperimetric glaucoma and control groups. Statistically significant differences were found for all GCC parameters, except for superior minus inferior GCC thickness. Statistically significant differences were also found for all full retinal parameters, except for superior minus inferior full retinal thickness. No statistically significant differences were found for outer retinal parameters. The three macular parameters with largest AUCs were GCC average thickness (0.79 ± 0.04), GCC inferior thickness (0.79 ± 0.05), and GCC superior thickness (0.76 ± 0.05). Pairwise comparisons did not show statistically significant differences between the AUCs of these parameters ($P > 0.05$ for all comparisons). The best GCC parameter, GCC average thickness, performed better than the best full retinal parameter, inferior full retinal thickness (0.79 vs. 0.70; $P = 0.009$), and the best outer retinal parameter, superior minus inferior outer retinal thickness (0.79 vs. 0.58; $P = 0.002$). The parameter with higher sensitivity at fixed specificity of 95% was GCC average thickness (43.8%). Figure 3 shows the ROC curves of the three macular parameters with largest AUCs.

Comparison of RNFL, ONH, and Macular Measurements

The RNFL parameter with largest AUC, average RNFL thickness, performed significantly better than the macular parameter with largest AUC, GCC average thickness (0.89 vs.

Table 1. Demographic and Clinical Characteristics of the Preperimetric Glaucoma and Control Study Groups

Characteristics	Preperimetric Glaucoma, $n = 48$	Control, $n = 94$	*P* Value
Age, y	65.9 ± 9.1	64.2 ± 11.2	0.427
% male	52.4	30.6	0.035
% African American	16.7	4.1	0.108
MD, dB	−0.81 (−1.82, −0.80, 0.12)	0.02 (−0.64, 0.25, 0.83)	0.001
PSD, dB	1.75 (1.46, 1.70, 1.84)	1.63 (1.29, 1.58, 1.81)	0.049
Follow-up, y	13.6 ± 4.2	12.8 ± 3.6	0.297

MD, mean deviation; PSD, pattern standard deviation.

0.79; $P = 0.007$), for differentiating between the preperimetric glaucoma and control groups. The average RNFL thickness also performed significantly better than the ONH parameter with largest AUC, vertical cup-to-disc ratio (0.89 vs. 0.74; $P = 0.015$). No statistically significant difference was found between vertical cup-to-disc ratio and GCC inferior thickness (0.79 vs. 0.74; $P = 0.46$). Figure 4 shows the ROC curves for the parameters with largest AUCs of each protocol.

Discussion

In the present study, we demonstrated that SDOCT RNFL assessment with the RTVue performed significantly better than ONH and macular assessments with the same instrument for detection of preperimetric glaucoma. To our knowledge, this is the first study that evaluated and compared the diagnostic accuracies of these measurements for detection of preperi-

Table 2. Mean ± SD Values of Peripapillary RNFL Thickness With AUC Curves and Sensitivities at Fixed Specificities for Discriminating Between Preperimetric Glaucoma and Control Groups

RNFL Thickness Parameter	Preperimetric Glaucoma, $n = 48$	Control, $n = 94$	*P* Value*	AUC (SE)	Sensitivity at 95% Specificity, %	Sensitivity at 80% Specificity, %
Average and quadrants						
Average	86.0 ± 7.6	99.5 ± 8.2	<0.001	0.89 (0.03)	70.8	79.2
Inferior hemisphere	85.7 ± 8.3	100.1 ± 9.0	<0.001	0.87 (0.03)	64.6	75.0
Inferior quadrant	104.9 ± 12.1	124.5 ± 13.5	<0.001	0.85 (0.03)	50.0	75.0
Superior hemisphere	86.3 ± 8.7	98.8 ± 9.4	<0.001	0.83 (0.03)	47.9	77.1
Superior quadrant	100.4 ± 11.0	116.0 ± 13.8	<0.001	0.81 (0.04)	43.8	53.2
Nasal quadrant	69.2 ± 11.5	78.6 ± 8.5	<0.001	0.75 (0.04)	45.8	58.3
Temporal quadrant	69.6 ± 9.8	78.7 ± 10.3	<0.001	0.73 (0.04)	29.2	45.8
45° sectors						
IT	111.4 ± 18.1	136.4 ± 17.2	<0.001	0.83 (0.03)	43.8	68.8
ST	106.7 ± 14.5	127.5 ± 16.8	<0.001	0.81 (0.03)	45.8	68.8
NU	73.2 ± 12.0	82.8 ± 9.9	<0.001	0.74 (0.04)	33.3	62.5
NL	65.2 ± 12.3	74.4 ± 9.0	<0.001	0.73 (0.04)	43.8	52.1
IN	98.5 ± 14.4	112.6 ± 18.6	<0.001	0.72 (0.04)	20.8	52.1
TU	71.3 ± 10.8	80.4 ± 11.5	<0.001	0.72 (0.04)	16.7	52.1
TL	67.9 ± 10.7	77.0 ± 11.8	<0.001	0.71 (0.04)	22.9	37.5
SN	94.1 ± 14.3	104.6 ± 14.5	<0.001	0.70 (0.04)	33.3	54.2
22.5° sectors						
IT1	119.6 ± 18.4	145.4 ± 18.9	<0.001	0.82 (0.03)	41.7	64.6
ST2	105.0 ± 19.0	129.2 ± 18.7	<0.001	0.81 (0.04)	41.7	64.6
TU2	77.6 ± 11.9	91.3 ± 14.7	<0.001	0.77 (0.04)	39.6	60.4
IT2	103.1 ± 22.3	127.4 ± 23.0	<0.001	0.77 (0.04)	31.9	60.4
NU1	64.1 ± 11.1	72.6 ± 8.1	<0.001	0.74 (0.05)	39.6	62.5
NU2	82.2 ± 14.4	93.0 ± 13.7	<0.001	0.73 (0.04)	27.1	58.3
NL2	69.2 ± 14.2	79.0 ± 11.0	<0.001	0.73 (0.04)	20.8	54.2
NL1	61.2 ± 11.7	69.8 ± 8.7	<0.001	0.72 (0.05)	33.3	52.1
TL2	72.5 ± 12.3	84.6 ± 15.9	<0.001	0.72 (0.04)	25.0	45.8
ST1	108.4 ± 17.2	125.7 ± 22.8	<0.001	0.72 (0.04)	12.5	43.8
IN1	104.8 ± 17.2	121.5 ± 22.4	<0.001	0.71 (0.04)	14.6	50.0
SN2	96.5 ± 15.4	107.3 ± 15.8	0.001	0.69 (0.05)	25.0	43.8
SN1	91.8 ± 16.1	101.9 ± 16.2	0.002	0.68 (0.05)	27.1	54.2
IN2	92.1 ± 14.2	103.6 ± 17.2	<0.001	0.68 (0.05)	23.4	39.6
TL1	63.3 ± 10.9	69.4 ± 10.9	0.003	0.65 (0.05)	18.8	39.6
TU1	65.0 ± 11.6	69.5 ± 10.9	0.035	0.59 (0.05)	22.9	25.0

IT, inferotemporal; ST, superotemporal; NL, lower nasal; NU, upper nasal; IN, inferonasal; SN, superonasal; TL, lower temporal; TU, upper temporal.

* For comparison of mean values of peripapillary retinal nerve fiber layer parameters between preperimetric glaucoma and control groups.

Investigative Ophthalmology & Visual Science

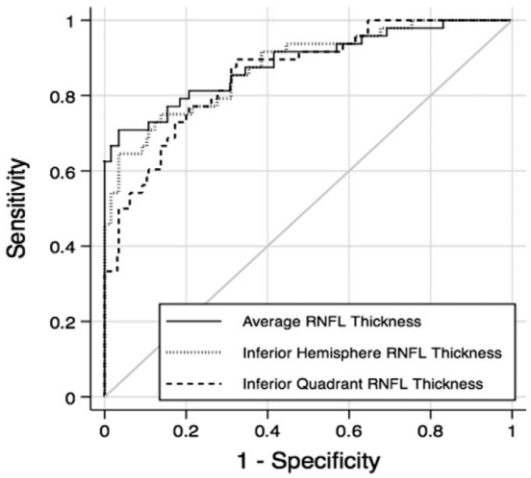

Figure 1. ROC curves for the three RNFL parameters with largest areas under the ROC curves: average RNFL thickness, inferior hemisphere RNFL thickness, and inferior quadrant RNFL thickness.

metric damage in a cohort of patients suspected of having glaucoma.

Several previous studies have evaluated the performance of SDOCT to detect glaucomatous damage.[6–10] Most of these studies have used visual field loss as the reference standard for classifying eyes as glaucomatous. That is, patients in these studies have been primarily selected based on the presence of clearly defined repeatable glaucomatous visual field loss, whereas controls were subjects without visual field damage or other suspicious findings for the disease. These studies are important for an initial evaluation of an instrument that is being considered as a potential diagnostic tool. In other words, if the instrument fails to differentiate patients with clearly defined disease versus those without any suspicious findings of damage, it will generally be considered inappropriate for diagnostic purposes. However, if the test succeeds at this stage, further steps are necessary in order to evaluate its capacity to provide relevant information that could be helpful in real clinical scenarios. Ancillary tests are used when there is diagnostic uncertainty, that is, in patients who are suspected of having the disease, not in those with clearly established diagnoses. In fact, in the absence of diagnostic uncertainty, no further diagnostic testing should be necessary. The presence of repeatable glaucomatous visual field damage obviates the need for performing a potentially costly imaging evaluation for diagnosing the disease, as the diagnosis will be already clear. To assess the potential of imaging devices as ancillary diagnostic tests, one needs to evaluate their performance in the presence of diagnostic uncertainty. We included a cohort of patients suspected of having glaucoma in our study and it should be noted that, at the time of imaging assessment, cases and controls were indistinguishable based on results of commonly performed clinical examinations, such as clinical optic disc evaluation and visual field assessment. This situation characterizes the presence of diagnostic uncertainty and the need for an additional test to assist in clarifying the diagnosis. By applying this design, the estimates of accuracy provided in our study are more likely to correspond to the real performance of imaging tests when used to diagnose glaucoma in clinical practice, compared with estimates of accuracy provided by previous studies.[6–10]

The AUCs reported in our study were considerably lower than the ones reported in previous studies that evaluated the diagnostic ability of SDOCT in glaucoma.[6–10] That can be explained by the less advanced stage of the disease of eyes included in the preperimetric glaucomatous group. In addition, the decreased performance is also related to the selection criteria of the control eyes, which had suspicious appearance of the optic disc. In a recent study by Rao et al.,[19] the ability of most SDOCT parameters in detecting glaucoma decreased significantly when evaluated against a clinically relevant control group that had suspicious appearance of the optic disc. The inclusion criteria used in our study selected a more homogeneous cohort, making it more difficult for the imaging test to differentiate similar groups frequently found in the clinical practice.

RNFL measurements performed significantly better than optic disc measurements in our study. This finding indicates that in the presence of suspicious optic disc appearance, RNFL assessment seems to be more useful than optic disc topographic measurements to establish the diagnosis. This may be directly related to the way that patients are identified as suspected of having glaucoma. As the evaluation of RNFL integrity during clinical examination or in stereophotographs is frequently difficult, most of these eyes are identified as suspects because of the presence of suspicious rim narrowing or enlarged optic disc cups. In this situation, it is not surprising that RNFL assessment provides more additional information for establishing the definitive diagnosis than further evaluation of optic disc rim and cup features by topographic parameters. It should be noted that the way eyes were identified as suspects for inclusion in our study resembles the way they are identified

Table 3. Mean ± SD Values of ONH With AUC Curves and Sensitivities at Fixed Specificities for Discriminating Between Preperimetric Glaucoma and Control Groups

ONH Parameter	Preperimetric Glaucoma, $n = 48$	Control, $n = 94$	*P* Value*	AUC (SE)	Sensitivity at 95% Specificity, %	Sensitivity at 80% Specificity, %
Vertical cup-to-disc ratio	0.79 ± 0.15	0.66 ± 0.19	0.001	0.74 (0.04)	18.8	56.3
Rim area, mm^2	0.66 ± 0.31	0.93 ± 0.32	<0.001	0.72 (0.05)	27.1	52.1
Rim volume, mm^3	0.06 ± 0.06	0.11 ± 0.09	0.001	0.72 (0.05)	27.1	52.1
Nerve head volume, mm^3	0.12 ± 0.10	0.21 ± 0.14	0.001	0.72 (0.05)	27.1	52.1
Cup-to-disc area ratio	0.59 ± 0.21	0.45 ± 0.20	0.001	0.66 (0.05)	27.1	41.7
Horizontal cup-to-disc ratio	0.81 ± 0.19	0.72 ± 0.22	0.025	0.63 (0.05)	20.9	41.7
Cup volume, mm^3	0.34 ± 0.29	0.21 ± 0.20	0.016	0.63 (0.06)	12.5	37.5
Cup area, mm^2	1.07 ± 0.50	0.83 ± 0.46	0.017	0.62 (0.06)	22.9	33.3
Disc area, mm^2	1.73 ± 0.33	1.76 ± 0.35	0.682	0.51 (0.06)	8.3	22.9

* For comparison of mean values of ONH parameters between preperimetric glaucoma and control groups.

Investigative Ophthalmology & Visual Science

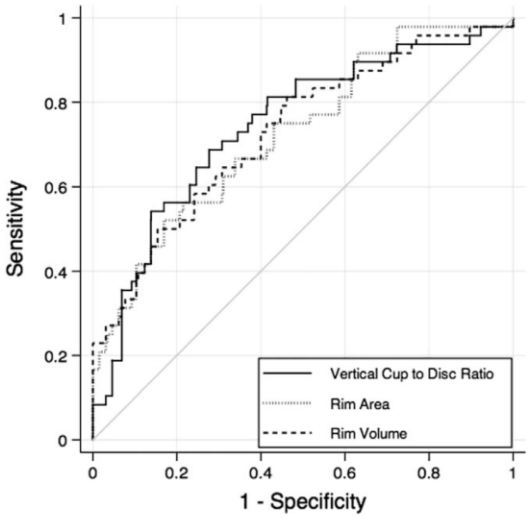

FIGURE 2. ROC curves the three ONH parameters with largest areas under the ROC curves: vertical cup-to-disc ratio, rim area, and rim volume.

as suspects in clinical practice (i.e., by clinical evaluation of photographs or fundoscopic examination at the slit-lamp). The worse performance of ONH compared with RNFL parameters could also reflect a weaker performance of the software in detecting topographic optic disc abnormalities. The ONH algorithm uses a reference line 150 μm above the RPE to define the transition between cup and rim, not taking into account individual variability, such as shallow or tilted optic discs. Moreover, although all images were reviewed, this protocol is still subject to human error, as manual delineation and centralization of the optic disc may be necessary. Conversely, the RNFL algorithm does not depend on a reference plane and may be less susceptible to the influence of normal phenotypic variations. However, it is important to keep in mind that, although ONH parameters performed worse than RNFL, it is possible that information provided by the ONH measurements could still potentially improve the diagnostic performance of the instrument if combined with that derived from RNFL assessment. For example, in a previous study by Medeiros et al.[20] that used the time-domain OCT, the authors showed that the combined information provided by different scanning areas had a better diagnostic accuracy than the information of each scan area separately. Further studies should investigate this hypothesis using SDOCT in a cohort of patients suspected of having glaucoma.

Since Zeimer et al.[5] first suggested that macular measurements could be useful for glaucoma diagnosis, several studies have been performed to test the effectiveness of such measurements in the detection of glaucomatous damage.[6,21–27] Theoretically, macular parameters have some advantages over RNFL parameters for glaucoma diagnosis. The macula has the highest concentration of ganglion cells in the retina and, therefore, loss of these cells could potentially be more readily detected at this region. Moreover, previous studies evaluating the time-domain OCT suggested that macular scans are more reproducible than RNFL scans.[28] This can be explained by the fact that RNFL scanning requires correct positioning of the scan circle by the operator and any misalignment tends to produce changes in RNFL measurements. Conversely, macular scans require internal fixation and are less dependent on the operator, which increases scan reproducibility.[29,30] Indeed, some studies showed that macular measurements are similar or even slightly better than RNFL measurements for glaucoma diagnosis.[22,25–27] However, our results did not show the same tendency, as RNFL measurements performed significantly better than macular measurements. The best macular parameter, GCC average thickness, had a considerably smaller AUC when compared with the best RNFL parameter. Moreover, in

TABLE 4. Mean ± SD Values of Macular Parameters With AUC Curves and Sensitivities at Fixed Specificities for Discriminating Between Preperimetric Glaucoma and Control Groups

Macular Parameters	Preperimetric Glaucoma, $n = 48$	Control, $n = 94$	P Value*	AUC (SE)	Sensitivity at 95% Specificity, %	Sensitivity at 80% Specificity, %
GCC parameters						
Average thickness, μm	83.6 ± 7.2	91.2 ± 6.6	<0.001	0.79 (0.04)	43.8	58.3
Inferior thickness, μm	83.0 ± 7.8	91.3 ± 6.8	<0.001	0.79 (0.05)	31.3	66.7
Superior thickness, μm	84.1 ± 7.5	91.1 ± 6.9	<0.001	0.76 (0.05)	31.3	62.5
Root mean square, %	0.10 ± 0.03	0.08 ± 0.02	<0.001	0.67 (0.05)	12.5	41.7
Global loss volume, %	11.3 ± 8.5	6.3 ± 5.1	0.002	0.65 (0.06)	33.3	58.3
Focal loss volume, %	1.9 ± 2.0	1.00 ± 1.2	0.011	0.59 (0.06)	14.6	43.8
S-I thickness, μm	1.1 ± 5.4	−0.2 ± 3.6	0.148	0.55 (0.05)	14.6	33.3
Full retinal parameters						
Inferior thickness, μm	250.4 ± 11.9	258.3 ± 13.6	0.004	0.70 (0.06)	8.3	45.8
Average thickness, μm	252.5 ± 11.7	260.2 ± 13.9	0.006	0.69 (0.06)	6.3	35.4
Superior thickness, μm	254.7 ± 12.3	262.1 ± 14.7	0.011	0.67 (0.06)	8.3	31.3
S-I thickness, μm	4.3 ± 5.7	3.8 ± 4.8	0.637	0.53 (0.05)	12.5	31.3
Outer retinal parameters						
S-I thickness, μm	3.2 ± 2.8	4.0 ± 2.8	0.151	0.58 (0.05)	10.4	37.5
Superior thickness, μm	170.6 ± 7.8	171.0 ± 10.5	0.828	0.53 (0.06)	0.0	12.5
Average thickness, μm	169.0 ± 7.6	169.0 ± 10.0	0.994	0.52 (0.06)	0.0	12.5
Inferior thickness, μm	167.4 ± 7.8	166.0 ± 9.8	0.830	0.50 (0.06)	0.0	12.5

S-I, superior minus inferior.
* For comparison of mean values of macular parameters between preperimetric glaucoma and control groups.

Investigative Ophthalmology & Visual Science

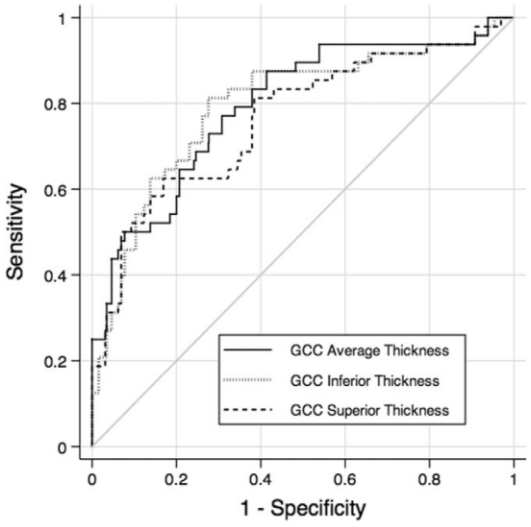

Figure 3. ROC curves for the three macular parameters with largest areas under the ROC curves: GCC average thickness, GCC inferior thickness, and GCC superior thickness.

Table 4 we can see that 6 of the 15 macular parameters were similar between preperimetric and control groups. It is also important to note that most of the studies that reported similar diagnostic performances between macular and RNFL parameters analyzed the SDOCT in a cohort of patients with more advanced stages of the disease. In advanced glaucoma, the macula has a higher chance of being involved and measurements at this region will probably be capable of detecting structural damage. Another possible explanation for the worse

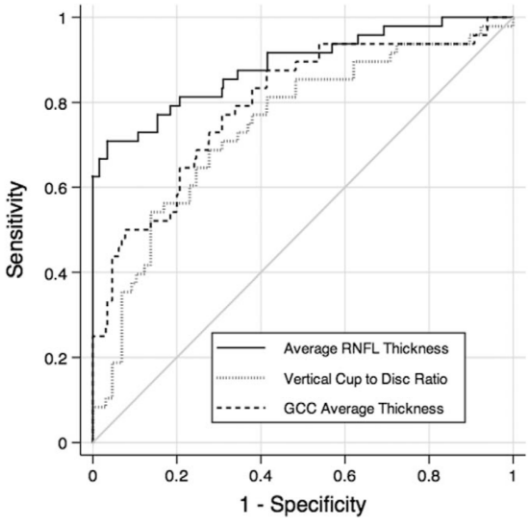

Figure 4. ROC curves for the parameters with largest AUCs of each protocol: inferior hemisphere RNFL thickness, vertical cup-to-disc ratio, and GCC retinal thickness.

performance of the GCC protocol is that the current algorithm available on the RTVue SDOCT does not differentiate the ganglion cell layer from the RNFL and internal limiting membrane. As nerve fibers from remote areas of the retina cross the area of macular scans, the ganglion cell layer thickness at a specific area might incorporate nerve fibers that do not correspond to the same affected area. It is possible that a segmentation algorithm that includes only the ganglion cell body layer could have better diagnostic performance than the one used in the current RTVue algorithm.

It is important to emphasize that the design used in our study evaluates only the situation of diagnosing preperimetric glaucoma in patients suspected of having the disease. Other study designs may be more relevant to evaluate the accuracy of SDOCT in other clinical scenarios. For example, if the study had the purpose of determining the ability of SDOCT to detect glaucomatous cases in situations of opportunistic screening, a design that contrasted patients with glaucoma versus unsuspected healthy eyes would have been more appropriate. Also, our design did not evaluate the ability of SDOCT to detect longitudinal changes. In fact, detection of progressive changes is usually the best way to clarify the diagnosis in eyes suspected of having glaucoma.[31] Further studies should evaluate the ability of the three scanning SDOCT areas to detect progressive damage in glaucoma suspects.

Longitudinal documentation of progressive disc damage was used in our study as the reference standard to obtain the final classification of eyes into cases and controls. Due to the wide variability of the optic disc appearances in the general population, a diagnosis of glaucoma cannot usually be made based on a single optic disc examination in eyes that do not show evidence of visual field loss. This study design enabled the evaluation of the performance of diagnostic tests in a scenario that resembles clinical practice and has been previously used in a similar situation.[11] However, it should be noted that this design might have some limitations. It might be argued that some patients from the control group could have developed glaucomatous optic disc damage or visual field defects after the end of the study and that the follow-up time was insufficient to detect them. Although it is unlikely that glaucoma patients would not progress or develop functional loss after having been followed untreated for almost 13 years, this possibility cannot be completely excluded. Another limitation of our study is that stereophotographic evaluation of the optic disc has an imperfect interobserver agreement.[32] As a consequence, some subjects could be misdiagnosed and incorrectly designated to the glaucomatous or to the control group. To minimize misclassifications, we required consensus grading by two expert ophthalmologists and a third experienced grader reviewed the stereophotographs in case of disagreement. Moreover, the use of progressive glaucomatous change as a reference standard requires longitudinal follow-up and serial documentation of the optic disc, which may not be available for all patients. Finally, difference in ancestry between groups was marginally significant in our study. Although previous studies reported that ancestry did not influence the diagnostic performance of the SDOCT technology,[33] we performed an additional analysis excluding black patients. As expected, similar results were achieved, with average RNFL thickness performing better than vertical cup-to-disc ratio (0.90 vs. 0.73; $P=0.009$) and GCC average thickness (0.90 vs. 0.80; $P=0.004$).

In conclusion, the results of this study demonstrated that SDOCT RNFL measurements performed significantly better than ONH and macular measurements in detecting preperimetric glaucomatous damage. Our results have significant implications for the use of the SDOCT technology for diagnosing structural damage in eyes suspected of having glaucoma. Future studies should evaluate whether a combina-

tion of different parameters can improve the performance of this technology to detect preperimetric glaucomatous damage.

Acknowledgments

Supported in part by National Institutes of Health/National Eye Institute Grants EY021818 (FAM), EY11008 (LMZ), and EY14267 (LMZ); Coordenação de Aperfeiçoamento de Pessoal de Nível Superior (CAPES) grant Bolsas no Exterior (BEX) 1066/11-0; an unrestricted grant from Research to Prevent Blindness (New York, New York); and grants for participants' glaucoma medications from Alcon, Allergan, Pfizer, Merck, and Santen.

Disclosure: **R. Lisboa**, None; **A. Paranhos Jr**, None; **R.N. Weinreb**, Alcon (C), Allergan (C), Bausch & Lomb (C), Carl Zeiss Meditec, Inc. (C), Nidek (S), Topcon (C), Aerie (S), Genentech (S); **L.M. Zangwill**, Carl Zeiss Meditec, Inc. (F), Heidelberg Engineering (F); **M.T. Leite**, None; **F.A. Medeiros**, Carl Zeiss Meditec, Inc. (F), Heidelberg Engineering (F)

References

1. Johnson CA, Sample PA, Zangwill LM, et al. Structure and function evaluation (SAFE): II. Comparison of optic disk and visual field characteristics. *Am J Ophthalmol*. 2003;135:148–154.
2. Johnson CA, Cioffi GA, Liebmann JR, Sample PA, Zangwill LM, Weinreb RN. The relationship between structural and functional alterations in glaucoma: a review. *Semin Ophthalmol*. 2000;15:221–233.
3. Harwerth RS, Carter-Dawson L, Smith EL III, Barnes G, Holt WF, Crawford ML. Neural losses correlated with visual losses in clinical perimetry. *Invest Ophthalmol Vis Sci*. 2004;45:3152–3160.
4. Medeiros FA, Zangwill LM, Bowd C, Mansouri K, Weinreb RN. The structure and function relationship in glaucoma: implications for detection of progression and measurement of rates of change. *Invest Ophthalmol Vis Sci*. 2012;53:6939–6946.
5. Zeimer R, Asrani S, Zou S, Quigley H, Jampel H. Quantitative detection of glaucomatous damage at the posterior pole by retinal thickness mapping. A pilot study. *Ophthalmology*. 1998;105:224–231.
6. Rao HL, Zangwill LM, Weinreb RN, Sample PA, Alencar LM, Medeiros FA. Comparison of different spectral domain optical coherence tomography scanning areas for glaucoma diagnosis. *Ophthalmology*. 2010;117:1692–1699, 1699.e1.
7. Leite MT, Rao HL, Zangwill LM, Weinreb RN, Medeiros FA. Comparison of the diagnostic accuracies of the Spectralis, Cirrus, and RTVue optical coherence tomography devices in glaucoma. *Ophthalmology*. 2011;118:1334–1339.
8. Park SB, Sung KR, Kang SY, Kim KR, Kook MS. Comparison of glaucoma diagnostic Capabilities of Cirrus HD and Stratus optical coherence tomography. *Arch Ophthalmol*. 2009;127:1603–1609.
9. Leung CK, Lam S, Weinreb RN, et al. Retinal nerve fiber layer imaging with spectral-domain optical coherence tomography: analysis of the retinal nerve fiber layer map for glaucoma detection. *Ophthalmology*. 2010;117:1684–1691.
10. Wang X, Li S, Fu J, et al. Comparative study of retinal nerve fibre layer measurement by RTVue OCT, GDx VCC. *Br J Ophthalmol*. 2011;95:509–513.
11. Medeiros FA, Zangwill LM, Bowd C, Sample PA, Weinreb RN. Use of progressive glaucomatous optic disk change as the reference standard for evaluation of diagnostic tests in glaucoma. *Am J Ophthalmol*. 2005;139:1010–1018.
12. Medeiros FA, Vizzeri G, Zangwill LM, Alencar LM, Sample PA, Weinreb RN. Comparison of retinal nerve fiber layer and optic disc imaging for diagnosing glaucoma in patients suspected of having the disease. *Ophthalmology*. 2008;115:1340–1346.
13. Medeiros FA. How should diagnostic tests be evaluated in glaucoma? *Br J Ophthalmol*. 2007;91:273–274.
14. Medeiros FA, Ng D, Zangwill LM, Sample PA, Bowd C, Weinreb RN. The effects of study design and spectrum bias on the evaluation of diagnostic accuracy of confocal scanning laser ophthalmoscopy in glaucoma. *Invest Ophthalmol Vis Sci*. 2007;48:214–222.
15. Lisboa R, Leite MT, Zangwill LM, Tafreshi A, Weinreb RN, Medeiros FA. Diagnosing preperimetric glaucoma with spectral domain optical coherence tomography. *Ophthalmology*. 2012;119:2261–2269.
16. Pepe M, Longton G, Janes H. Estimation and comparison of receiver operating characteristic curves. *Stata J*. 2009;9:1.
17. Zhou X-H, Obuchowski NA, McClish DK. Analysis of correlated ROC data. In: Zhou X-H, Obuchowski NA, McClish DK, eds. *Statistical Methods in Diagnostic Medicine*. New York: Wiley; 2002:274–306.
18. Alonzo TA, Pepe MS. Distribution-free ROC analysis using binary regression techniques. *Biostatistics*. 2002;3:421–432.
19. Rao HL, Kumbar T, Addepalli UK, et al. Effect of spectrum bias on the diagnostic accuracy of spectral-domain optical coherence tomography in glaucoma. *Invest Ophthalmol Vis Sci*. 2012;53:1058–1065.
20. Medeiros FA, Zangwill LM, Bowd C, Vessani RM, Susanna R Jr, Weinreb RN. Evaluation of retinal nerve fiber layer, optic nerve head, and macular thickness measurements for glaucoma detection using optical coherence tomography. *Am J Ophthalmol*. 2005;139:44–55.
21. Ojima T, Tanabe T, Hangai M, Yu S, Morishita S, Yoshimura N. Measurement of retinal nerve fiber layer thickness and macular volume for glaucoma detection using optical coherence tomography. *Jpn J Ophthalmol*. 2007;51:197–203.
22. Leung CK, Chan WM, Yung WH, et al. Comparison of macular and peripapillary measurements for the detection of glaucoma: an optical coherence tomography study. *Ophthalmology*. 2005;112:391–400.
23. Tan O, Li G, Lu AT, Varma R, Huang D. Mapping of macular substructures with optical coherence tomography for glaucoma diagnosis. *Ophthalmology*. 2008;115:949–956.
24. Ishikawa H, Stein DM, Wollstein G, Beaton S, Fujimoto JG, Schuman JS. Macular segmentation with optical coherence tomography. *Invest Ophthalmol Vis Sci*. 2005;46:2012–2017.
25. Moreno PA, Konno B, Lima VC, et al. Spectral-domain optical coherence tomography for early glaucoma assessment: analysis of macular ganglion cell complex versus peripapillary retinal nerve fiber layer. *Can J Ophthalmol*. 2011;46:543–547.
26. Seong M, Sung KR, Choi EH, et al. Macular and peripapillary retinal nerve fiber layer measurements by spectral domain optical coherence tomography in normal-tension glaucoma. *Invest Ophthalmol Vis Sci*. 2010;51:1446–1452.
27. Nakatani Y, Higashide T, Ohkubo S, Takeda H, Sugiyama K. Evaluation of macular thickness and peripapillary retinal nerve fiber layer thickness for detection of early glaucoma using spectral domain optical coherence tomography. *J Glaucoma*. 2011;20:252–259.
28. Gurses-Ozden R, Teng C, Vessani R, Zafar S, Liebmann JM, Ritch R. Macular and retinal nerve fiber layer thickness measurement reproducibility using optical coherence tomography (OCT-3). *J Glaucoma*. 2004;13:238–244.
29. Vizzeri G, Bowd C, Medeiros FA, Weinreb RN, Zangwill LM. Effect of signal strength and improper alignment on the variability of stratus optical coherence tomography retinal nerve fiber layer thickness measurements. *Am J Ophthalmol*. 2009;148:249–255.e1.
30. Schuman JS, Pedut-Kloizman T, Hertzmark E, et al. Reproducibility of nerve fiber layer thickness measurements using optical coherence tomography. *Ophthalmology*. 1996;103:1889–1898.

31. Medeiros FA, Alencar LM, Zangwill LM, Bowd C, Sample PA, Weinreb RN. Prediction of functional loss in glaucoma from progressive optic disc damage. *Arch Ophthalmol*. 2009;127:1250–1256.
32. Breusegem C, Fieuws S, Stalmans I, Zeyen T. Agreement and accuracy of non-expert ophthalmologists in assessing glaucomatous changes in serial stereo optic disc photographs. *Ophthalmology*. 2011;118:742–746.
33. Girkin CA, Liebmann J, Fingeret M, Greenfield DS, Medeiros F. The effects of race, optic disc area, age, and disease severity on the diagnostic performance of spectral-domain optical coherence tomography. *Invest Ophthalmol Vis Sci*. 2011;52:6148–6153.

Investigative Ophthalmology & Visual Science

2.3. Likelihood Ratios for Glaucoma Diagnosis Using Spectral-Domain Optical Coherence Tomography

Renato Lisboa, MD; Kaweh Mansouri, MD; Linda M. Zangwill, PhD; Robert N. Weinreb, MD; Felipe A. Medeiros, MD, PhD.

American Journal of Ophthalmology, 2013 Nov; 156(5): 918-26

Likelihood Ratios for Glaucoma Diagnosis Using Spectral-Domain Optical Coherence Tomography

RENATO LISBOA, KAWEH MANSOURI, LINDA M. ZANGWILL, ROBERT N. WEINREB, AND FELIPE A. MEDEIROS

• PURPOSE: To present a methodology for calculating likelihood ratios for glaucoma diagnosis for continuous retinal nerve fiber layer (RNFL) thickness measurements from spectral-domain optical coherence tomography (spectral-domain OCT).
• DESIGN: Observational cohort study.
• METHODS: A total of 262 eyes of 187 patients with glaucoma and 190 eyes of 100 control subjects were included in the study. Subjects were recruited from the Diagnostic Innovations Glaucoma Study. Eyes with preperimetric and perimetric glaucomatous damage were included in the glaucoma group. The control group was composed of healthy eyes with normal visual fields from subjects recruited from the general population. All eyes underwent RNFL imaging with Spectralis spectral-domain OCT. Likelihood ratios for glaucoma diagnosis were estimated for specific global RNFL thickness measurements using a methodology based on estimating the tangents to the receiver operating characteristic (ROC) curve.
• RESULTS: Likelihood ratios could be determined for continuous values of average RNFL thickness. Average RNFL thickness values lower than 86 μm were associated with positive likelihood ratios (ie, likelihood ratios greater than 1), whereas RNFL thickness values higher than 86 μm were associated with negative likelihood ratios (ie, likelihood ratios smaller than 1). A modified Fagan nomogram was provided to assist calculation of posttest probability of disease from the calculated likelihood ratios and pretest probability of disease.
• CONCLUSION: The methodology allowed calculation of likelihood ratios for specific RNFL thickness values. By avoiding arbitrary categorization of test results, it potentially allows for an improved integration of test results into diagnostic clinical decision making. (Am J Ophthalmol 2013;■:■–■. © 2013 by Elsevier Inc. All rights reserved.)

AJO.com Supplemental Material available at AJO.com.
Accepted for publication Jun 12, 2013.
From Hamilton Glaucoma Center, Department of Ophthalmology, University of California San Diego, La Jolla, California.
Inquiries to Felipe A. Medeiros, Hamilton Glaucoma Center, University of California, San Diego, 9500 Gilman Drive, La Jolla, CA 92093; e-mail: fmedeiros@glaucoma.ucsd.edu

SEVERAL IMAGING TECHNOLOGIES HAVE BEEN INTRODUCED with the purpose of objectively quantifying structural damage to the optic disc and retinal nerve fiber layer (RNFL) in glaucoma. As the number of available technologies increases, difficult decisions arise about which tests should be used and how to incorporate their results in clinical practice. Sensitivity, specificity, and the area under the receiver operating characteristic (ROC) curve have traditionally been used as measures of diagnostic accuracy. Although well established, these measures have some limitations in clinical use, which arise mainly from the fact that they are population measures; that is, they summarize the characteristics of the test over a population. However, in the diagnostic process, clinicians want measures that can be directly incorporated into the decision-making process for individual patients.

During the diagnostic process, a clinician combines medical history and clinical examination to estimate the probability that the disease is present. If there is still uncertainty with regard to the presence of disease, additional diagnostic tests can be performed. The purpose of the diagnostic test will be to modify the pretest probability of disease into a more conclusive posttest probability of disease. Diagnostic likelihood ratios can be directly used to modify the initial suspicion for disease (pretest probability) into a new probability of disease (posttest probability). The use of likelihood ratios has been proposed as the best way of incorporating results of diagnostic tests into clinical decision making according to the principles of evidence-based medicine.[1] Moreover, like sensitivity and specificity, likelihood ratios have the property of not being affected by the prevalence of the disease.

A few previous studies have reported likelihood ratios for glaucoma diagnosis using optic disc and RNFL analysis from imaging instruments.[2–5] In these studies, results of the diagnostic tests were arbitrarily categorized into normal vs abnormal according to specific cut-offs. The dichotomization of test results with continuous outcomes may result in loss of information, because results that are markedly abnormal are grouped with results that are only mildly abnormal.[6–10] The loss of information is even more important when the patient's test result is close to the established cut-off.[6]

In the present study, we apply a methodology for estimating likelihood ratios for glaucoma diagnosis that does not require arbitrary categorization of test results. This

0002-9394/$36.00
http://dx.doi.org/10.1016/j.ajo.2013.06.017

methodology allows the calculation of likelihood ratios for all values of the test with direct application to the calculation of posttest probability of disease. We demonstrate the methodology using RNFL thickness analysis with spectral-domain optical coherence tomography (spectral-domain OCT). Finally, we propose a modified Fagan nomogram that can be used to facilitate the use of likelihood ratios for continuous RNFL thickness measurements into the diagnostic process at the clinical practice.

METHODS

THIS WAS AN OBSERVATIONAL COHORT STUDY. PATIENTS were recruited from the Diagnostic Innovations in Glaucoma Study conducted at the Hamilton Glaucoma Center (University of California, San Diego). The Diagnostic Innovations in Glaucoma Study is registered at http://www.clinicaltrials.gov under the identifier NCT00221897. Participants were longitudinally evaluated according to a protocol that included visits with a comprehensive clinical examination and several imaging and functional tests. All participants who met the inclusion criteria described below were enrolled and all data were entered in a computer database. Informed consent was obtained from all participants. The University of California San Diego Human Subjects Committee approved all protocols, and methods adhered to the Declaration of Helsinki.

Each subject underwent a comprehensive ophthalmic examination, including review of medical history, best-corrected visual acuity, slit-lamp biomicroscopy, intraocular pressure measurement using Goldmann applanation tonometry, gonioscopy, dilated fundoscopy examination using a 78-diopter (D) lens, stereoscopic optic disc photography, and standard automated perimetry with 24-2 Swedish Interactive Threshold Algorithm (Carl Zeiss Meditec, Inc, Dublin, California, USA). To be included, subjects had to have best-corrected visual acuity of 20/40 or better, spherical refraction within ±5.0 D, cylinder correction less than 3.0 D, and open angle with gonioscopy. Subjects with coexisting retinal disease, uveitis, or nonglaucomatous optic disc neuropathy were excluded from the study.[11]

Eyes were classified as glaucomatous if they had repeatable (at least 3 consecutive) abnormal visual field test results, defined as pattern standard deviation with a P value <5% and/or a glaucoma hemifield test result outside normal limits, regardless of the appearance of the optic disc. Visual fields with more than 33% fixation losses, more than 33% false-negative errors, or more than 15% false-positive errors were excluded. The only exception was the inclusion of patients with more than 33% of false-negative errors and advanced disease stage (mean deviation lower than minus 12 dB). In addition, all visual fields were reviewed by the Visual Field Assessment Center (University of California at San Diego) and masked to the results of other tests.[11] Visual fields were reviewed and excluded in the presence of artifacts such as eyelid or rim artifacts, fatigue effects, inattention, or inappropriate fixation. Visual fields were also reviewed for the presence of abnormalities that could indicate diseases other than glaucoma, such as homonymous hemianopia.

We also included in the glaucoma group patients with preperimetric glaucomatous damage. The inclusion of these eyes required longitudinal follow-up to determine their ultimate diagnosis, as described in previous publications.[12–16] These eyes had normal visual field examinations at the time of imaging, but had history of documented evidence of progressive glaucomatous change in the appearance of the optic disc, as assessed by simultaneous stereoscopic photographs (Topcon Instrument Corporation of America, Paramus, New Jersey, USA). The evidence of progressive glaucomatous damage had to be present before the imaging test date. For evaluation of progressive optic disc damage, stereoscopic sets were examined using a stereoscopic viewer (Asahi; Pentax, Tokyo, Japan). All stereophotographs were evaluated by 2 experienced graders masked to the subject's identity, chronological sequence of the stereophotographs, and other test results. For inclusion, stereophotographs needed to be graded adequate or better. Definition of change was based on focal or diffuse thinning of the neuroretinal rim, increased excavation, or enlargement of the RNFL defects. Changes on rim color, presence of disc hemorrhages, or progressive peripapillary atrophy were not sufficient for characterization of progression. Discrepancies between the 2 graders were resolved by either consensus or adjudication of a third experienced grader. The use of this composite reference standard for glaucoma diagnosis allowed us to evaluate likelihood ratios for continuous RNFL thickness measurements in patients with a broad spectrum of disease severity, as patients with visual field loss and patients with normal visual fields but confirmed progressive glaucomatous damage were included.

Healthy eyes had intraocular pressures of 21 mm Hg or less with no history of increased intraocular pressure, a normal clinical examination, and at least 2 reliable baseline normal visual field tests. A normal visual field was defined as a mean deviation and pattern standard deviation within 95% confidence limits and a glaucoma hemifield test result within normal limits. Healthy subjects were recruited from the general population or from spouses and relatives of patients.

• **SPECTRALIS SPECTRAL-DOMAIN OCT:** RNFL thickness measurements were obtained using the Spectralis spectral-domain OCT (software version 5.3.3.0; Heidelberg Engineering, Carlsbad, California, USA). Details of its operation have been published elsewhere.[17–19] The high-resolution protocol was used, obtaining 1536 A-scans from a 3.45-mm circle centered at the optic disc, providing an axial resolution of 3.9 μm and a lateral resolution of 6.0 μm. To increase the image quality, the Spectralis

spectral-domain OCT includes an automatic real-time function that gathers multiple frames (B-scans). On average, 20.0 B-scans per eye were used to generate the peripapillary RNFL curve. The images were then averaged for noise reduction. The quality score ranges from 0 dB (poor) to 40 dB (excellent). All images were reviewed by experienced technicians at the Imaging Data Evaluation and Assessment Center.[11] To be included, images had to be centered, with accurate segmentation, and had to have a signal strength >15 dB. For this study we estimated likelihood ratios for the global RNFL thickness (360-degree measure). We used this parameter because it represents a global measure of structural damage that has been shown to have good diagnostic performance in previous studies.[18,20]

• **STATISTICAL ANALYSIS:** Descriptive statistics included mean and standard deviation for normally distributed variables and mean, median, first quartile, and third quartile for non-normally distributed variables (determined by the Kolmogorov-Smirnov normality test). Normally distributed variables were compared between groups using the 2-sample *t* test, while non-normally distributed variables were compared using the Wilcoxon rank sum test. The χ^2 test was used to test for differences in categorical variables between groups. Generalized estimating equations with robust standard errors were used to adjust for potential correlations between both eyes of the same individual.

The application of likelihood ratios in the interpretation of results of imaging instruments for glaucoma diagnosis has been detailed previously.[2,3] Briefly, likelihood ratio is the ratio between 2 probabilities: the probability of a given test result when the disease is present (true-positive ratio) divided by the probability of the same test result when the disease is absent (false-positive ratio).[1,21] Once determined, a likelihood ratio can be directly incorporated into the calculation of posttest odds of disease by using a formulation of the Bayes theorem, which uses odds of disease.[22]

The first step in the calculation of the posttest probability of disease is to calculate the pretest odds of disease from the pretest probability of the disease using the following equation:

$$\text{odds} = \text{probability}/(1 - \text{probability}) \quad (1)$$

Then, the likelihood ratio can be used to modify the pretest odds of disease into a new posttest odds of disease using this equation:

$$\text{posttest odds} = (\text{pretest odds}) \times \text{likelihood ratio} \quad (2)$$

From the above formula it can be seen that a likelihood ratio of 1 means that the test provides no additional information about the presence of disease, as the posttest odds will be equal to the pretest odds. Likelihood ratios higher or lower than 1 will increase or decrease the likelihood of disease, respectively.

Finally, we can calculate the posttest probability of disease from posttest odds of disease using the following equation:

$$\text{probability} = \text{odds}/(1 + \text{odds}) \quad (3)$$

Supplemental Figure 1 (available at AJO.com) shows the steps necessary for the calculation of the posttest probability of disease and how the modified Fagan nomogram[22] (described below) simplifies the process.

In the present study, likelihood ratios for continuous RNFL thickness values were estimated using the method described by Gu and Pepe.[23] Formulas used to derive likelihood ratios for continuous RNFL thickness measurements are included in the Appendix.[24–31] Supplemental Figure 2 (available at AJO.com) illustrates that the likelihood ratio can be interpreted as the tangent of the ROC curve at a threshold *c*. Adjustments for the presence of both eyes and for differences in confounding variables (age and sex) between cases and controls were performed as described by Alonzo and Pepe.[27]

All statistical analyses were performed with commercially available software (Stata version 11; StataCorp, College Station, Texas, USA). The alpha level (type I error) was set at 0.05.

RESULTS

THE STUDY INCLUDED 262 EYES OF 187 PATIENTS WITH GLAUCOMA and 190 eyes of 100 control subjects. The Table shows demographic and clinical characteristics of the included subjects. Patients in the glaucoma group were significantly older than the subjects in the control group. In addition, there were more male patients in the glaucoma group. Glaucomatous eyes had, on average, significantly thinner RNFLs when compared with the control group.

Figure 1 shows the relationship between global RNFL thickness and likelihood ratios greater than 1 (ie, likelihood ratios associated with increase in the probability of disease). As expected, the thinner the RNFL thickness measurement, the greater the associated likelihood ratio. Figure 2 shows the relationship between global RNFL thickness and likelihood ratios smaller than 1 (ie, likelihood ratios associated with decrease in the probability of disease). Thicker RNFL thickness measurements were associated with decreased likelihood ratios.

Figure 3 illustrates the relationship between posttest probability of disease and global RNFL thickness for arbitrary values of pretest probability of disease. Thinner RNFL values were associated with an increase in the posttest probability of disease. For example, as expected from Figure 3, a global RNFL thickness result of 70 μm would have a large effect on the probability of disease, modifying a pretest probability of disease from 30% to a new posttest probability of disease of 91%. For the same pretest probability of disease of 30%, a global RNFL thickness result of

TABLE. Demographic and Clinical Characteristics of the Glaucoma and Control Groups Included in the Study

Characteristic	Glaucoma (n = 262)	Control (n = 190)	*P* Value
Age, y[a]	70.5 ± 11.1	53.1 ± 17.2	<.001
Sex, % male	74.6	25.4	<.001
Ancestry, % African-American	67.1	32.9	.143
MD, dB[b]	−4.3 (−5.6, −2.4, −1.2)	0.4 (−0.4, 0.6, 1.2)	<.001
PSD, dB[b]	4.8 (2.1, 3.3, 7.5)	1.5 (1.3, 1.5, 1.7)	<.001
Global RNFL thickness, μm[a]	73 ± 15	97 ± 10	<.001

MD = mean deviation; PSD = pattern standard deviation; RNFL = retinal nerve fiber layer.
[a]Normally distributed variables; represented by mean (standard deviation).
[b]Non-normally distributed variables; represented by mean (first quartile, median, third quartile).

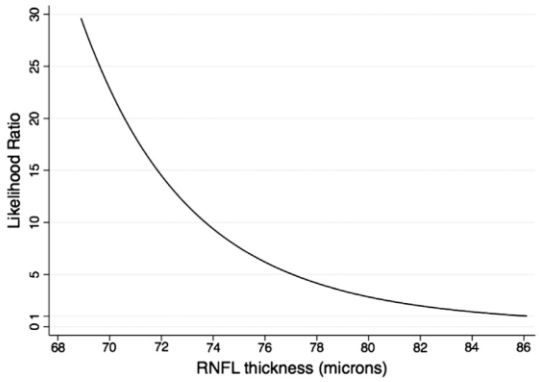

FIGURE 1. Relationship between likelihood ratios for glaucoma diagnosis and global retinal nerve fiber layer thickness measurements for likelihood ratios values greater than 1 (ie, associated with increased posttest probability of disease).

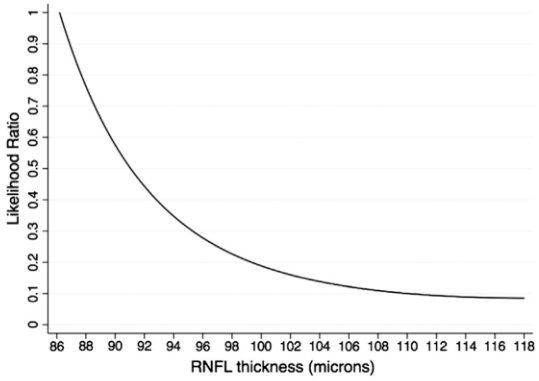

FIGURE 2. Relationship between likelihood ratios for glaucoma diagnosis and global retinal nerve fiber layer thickness measurements for likelihood ratios values smaller than 1 (ie, associated with decrease in the posttest probability of disease).

110 μm would result in a posttest probability of 4%, almost excluding the presence of disease. However, an intermediate RNFL thickness result of 85 μm would have an insignificant impact on the probability of disease, modifying the pretest probability of 30% to a similar posttest probability of 34%. Figure 4 illustrates the relationship between pretest and posttest probabilities of disease for arbitrary global RNFL thickness results of 70 μm, 85 μm, and 110 μm.

Figure 5 shows a modified Fagan nomogram,[22] where the likelihood ratios in the center column were replaced by the corresponding RNFL thickness values. This nomogram can be used for a straightforward estimation of the posttest probability of disease according to the pretest probability of disease and continuous values of global RNFL thickness. A line drawn from the pretest probability of disease in the left column through the RNFL thickness result in the center column gives the posttest probability of disease in the right column.

Figure 6 illustrates how likelihood ratios for continuous RNFL thickness measurements can be applied to the clinical practice with the help of the modified Fagan nomogram. After medical history, clinical examination, intraocular pressure, and visual field examination, the eye at the top was considered to have a pretest probability of 40%. However, after analyzing the results of the spectral-domain OCT we could see that the RNFL thickness was 67 μm. By applying the modified Fagan nomogram we calculated a higher posttest probability of 97%. On the other hand, the eye at the bottom was considered to have a pretest probability of 60%. After spectral-domain OCT results showing a RNFL measurement of 104 μm, and with the help of the Fagan nomogram, the posttest probability for glaucoma decreased to 18%.

DISCUSSION

IN THIS STUDY, WE REPORTED LIKELIHOOD RATIOS FOR continuous values of RNFL thicknesses provided by spectral-domain OCT. To the best of our knowledge, this is the first study to report likelihood ratios for continuous

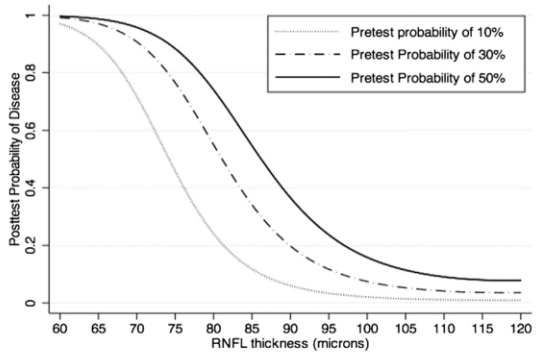

FIGURE 3. Relationship between posttest probability of disease for glaucoma diagnosis and retinal nerve fiber layer thicknesses.

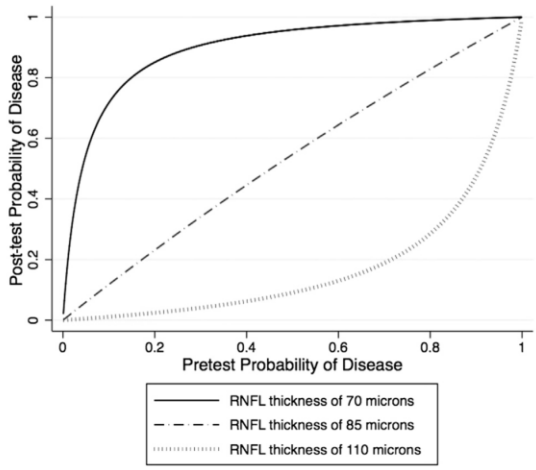

FIGURE 4. Relationship between posttest probability of disease for glaucoma diagnosis and pretest probability of disease.

values of a marker in glaucoma. Our results may have significant implications in the diagnostic process of glaucomatous damage, as specific posttest probabilities of disease can be assessed for individual values of RNFL thickness. Further, the methodology used in our study can be easily extended for calculation of likelihood ratios for other parameters and diagnostic tests.

Sensitivity and specificity have previously been used in several studies to report diagnostic accuracies of the spectral-domain OCT technology in glaucoma.[18,32–37] Sensitivity and specificity reflect the probability that a particular test result is positive or negative given the presence or the absence of the disease, respectively. However, knowledge of whether or not the disease is present would clearly obviate the auxiliary test. That is,

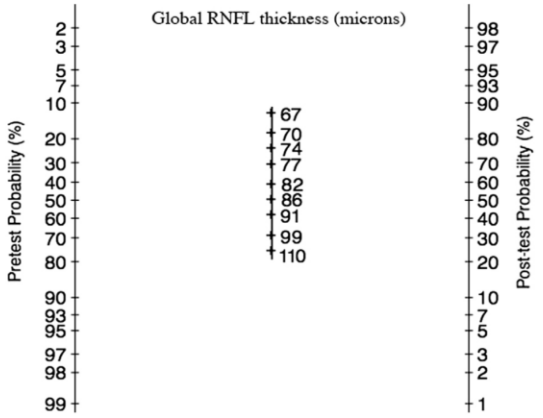

FIGURE 5. Modified Fagan nomogram for calculation of the posttest probability of glaucoma according to the pretest probability of glaucoma and continuous values of global retinal nerve fiber layer thickness.

we apply diagnostic tests in clinical practice to patients in which the disease status is unknown. Therefore, sensitivity and specificity offer limited application for direct interpretation of results of diagnostic tests in individual patients. Similarly, the area under the ROC curve is important to compare diagnostic accuracies of ancillary tests, but has little intuitive clinical meaning and offers little help when a clinician wants to evaluate test results for an individual patient. The starting point of the diagnostic process occurs when the clinician combines the medical history with clinical examination in order to estimate the probability of the presence of disease, also known as the pretest probability. Then the results of an ancillary test can be used to modify the pretest probability, yielding a new posttest probability of disease. In other words, the posttest probability is the revised probability of the disease after the knowledge of the diagnostic test result. Likelihood ratios can be used in a practical way to derive the posttest probability of disease by applying the formulas previously provided in the methods section. This allows direct incorporation of diagnostic test results into clinical decision making. For example, if a pretest probability of glaucoma in a patient suspected of having the disease is 50%, then by applying equation 1 we can calculate the pretest odds in favor of the disease, which would be $0.5/(1 - 0.5) = 1$. Let's then assume that this same patient has a global RNFL thickness result of 75 μm. From Figure 1 we can obtain a likelihood ratio of 8 for this result. By applying equation 2, the revised posttest odds of glaucoma would be $1 \times 8 = 8$. This posttest odds, by applying equation 3, corresponds to a probability of $8/(8 + 1) = 88\%$. Thus, the global RNFL thickness result has been used to revise an initial probability (pretest probability) of disease of 50% into a new probability (posttest

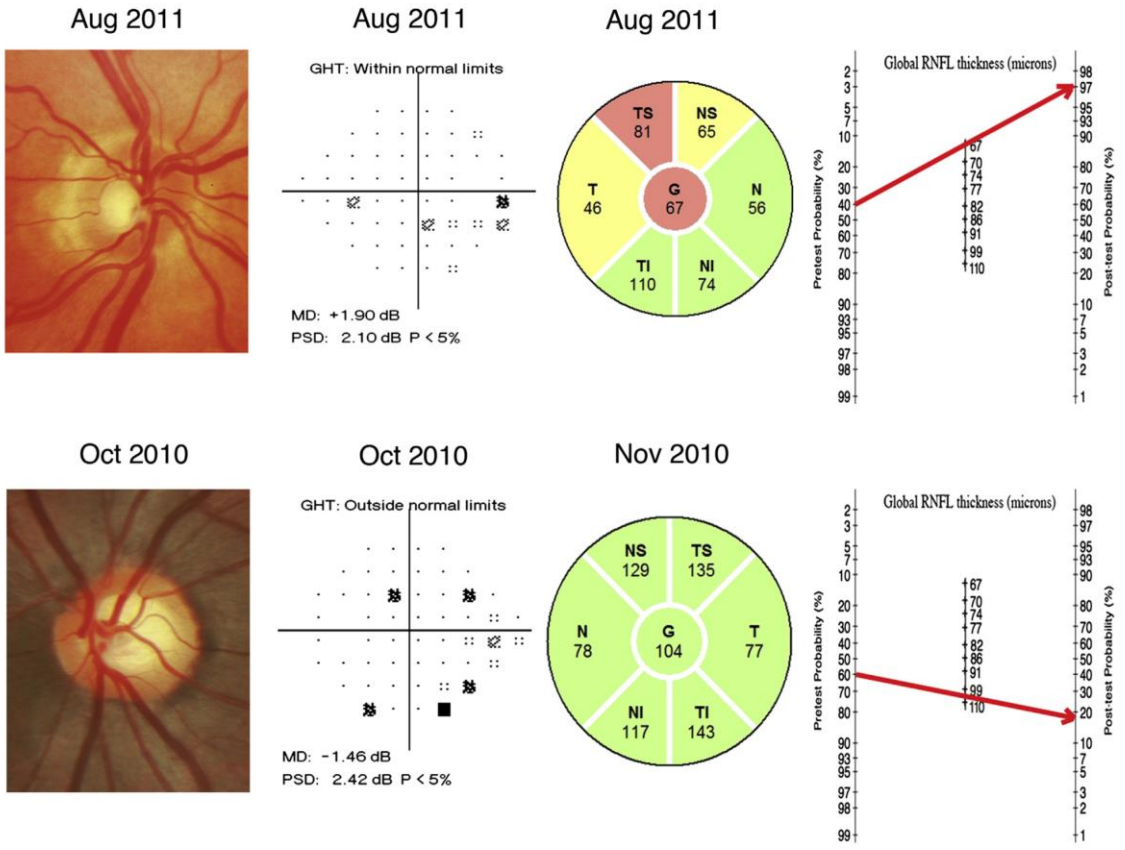

FIGURE 6. Examples of eyes included in the study illustrating the benefits of incorporating diagnostic likelihood ratios for continuous test results in the diagnostic process for glaucoma. Based on the medical history, clinical examination, intraocular pressure, and visual field examination, the eye at the top was considered to have a pretest probability of 40%. The spectral-domain OCT measured a retinal nerve fiber layer (RNFL) thickness of 67 μm. By applying the modified Fagan nomogram we can see that the posttest probability increased to 97%. Conversely, the eye at the bottom was considered to have a pretest probability of 60%. The spectral-domain OCT measured a RNFL thickness of 104 μm. By applying the modified Fagan nomogram the posttest probability decreased considerably to 18%.

probability) of 88%. In order to simplify the calculations exemplified above, the posttest probability of glaucoma for different global RNFL thicknesses can be directly inferred from the modified Fagan nomogram illustrated in Figure 5.

The printout of the Spectralis spectral-domain OCT displays classifications of RNFL thickness parameters according to comparisons to a normative database population. Although this categorization has the purpose of simplifying interpretation of results in clinical practice, it can lead to important loss of information and may cause distortions in the interpretation of test results, as widely different RNFL thickness values are potentially given the same diagnostic weight.[7–10] For example, using the conventional diagnostic approach, a clinician would classify an eye as abnormal if the measured RNFL thickness is below the 1% cut-off calculated from the distribution of values in the normative database. Such approach will lead to an "all-or-nothing" decision, which ignores that patients in identical categories may actually have very different probabilities of disease. Two eyes with RNFL thicknesses of 73 μm and 65 μm would both be categorized as outside normal limits using the conventional approach, with no distinction made between them, as both thicknesses would be below the 1% cut-off of the normal population (74 μm). However, considering the same pretest probability of 30% for both eyes, for example, the use of likelihood ratios for continuous RNFL thickness values would lead to different posttest probabilities of 83% and 97%. The same reasoning can be applied to eyes classified as within normal limits using the conventional approach. For example, 2 eyes with RNFL thicknesses of 81 μm and 110 μm would both

be categorized as within normal limits. However, considering the same pretest probability of 30% for both eyes, the use of likelihood ratios for continuous RNFL thickness values would lead to very different posttest probabilities of 51% and 5%. Clearly, these eyes should not be seen as having the same probability for the presence of the disease, as it would be implied by the conventional approach.

In a previous study, Medeiros and associates[2] reported likelihood ratios for arbitrarily defined cut-off intervals of RNFL thickness measurements from optical coherence tomography and scanning laser polarimetry. They found that thinner RNFL thickness measurements were associated with larger likelihood ratios. Our results are in agreement with this previous study. However, our investigation provides additional information by calculating likelihood ratios for continuous RNFL thickness measurements, avoiding any arbitrary categorization. Although our method requires some mathematical calculations, it could be easily implemented into standard software of imaging instruments so that clinicians would have direct availability to likelihood ratios and plots of posttest vs pretest probabilities of disease. This approach would provide clinicians with immediate information about the impact of a specific test result in changing the probability of disease.

Currently, there are no formal ways of calculating pretest probabilities in glaucoma diagnosis. An obvious pretest probability to consider would be the prevalence of the disease in the general population, but this could not be applicable to clinic-based populations. Therefore, calculations of pretest probabilities are still a subjective component of diagnostic evaluation and can vary substantially among physicians. As clinicians evaluate a patient suspected of having glaucoma, they measure the intraocular pressure, evaluate the optic nerve, and obtain visual field tests. If we fully knew the properties of each of these tests, one could move sequentially through them, incorporating each piece of information and continuously recalculating the probability of glaucoma, so that the posttest probability after one test would be the pretest probability before the other. In fact, clinicians do proceed in this way. However, because the formal properties (likelihood ratios) of these items are not available, they must rely on clinical experience and intuition to arrive at the pretest probability that precedes ordering a diagnostic test such as spectral-domain OCT. The correlation among the tests used in the diagnostic process is also an important consideration when using likelihood ratios. If the pretest probability before applying spectral-domain OCT was derived after using a diagnostic test that is highly correlated with spectral-domain OCT, this could affect the calculations of posttest probability using the results presented in our study. As the tests would not be independent, one could not simply multiply the pretest probability (obtained after applying the first test) to the likelihood ratio for the second test without taking into account their correlations. The use of multivariate approaches combining different tests may help overcome these limitations. Further studies should evaluate combined approaches for glaucoma diagnosis that could integrate spectral-domain OCT results with those of other medical tests.

In the present study, we used global RNFL thickness in order to provide a general description of our methodology for calculating likelihood ratios for different RNFL thickness values. Although global RNFL thickness has been described as having good accuracy for glaucoma diagnosis, it is likely that improved accuracy could be obtained by using sectoral RNFL thicknesses or combinations of parameters. Applications of likelihood ratio calculations for RNFL thickness measurements from sectors around the optic disc would have to take into account the interdependency among the values. A possible strategy would be to calculate an index combining sectoral measurements, such as in a linear discriminant function,[38] and then calculate likelihood ratios for this index. The same approach could potentially be used for combining results from multiple instruments. Finally, it should be emphasized that RNFL thickness measurements are not interchangeable between different commercially available spectral-domain OCTs.[17] As a consequence, specific results on likelihood ratios obtained for the Spectralis should not be extrapolated to other spectral-domain OCTs and calculations of likelihood ratios should be done for each instrument.

The cross-sectional design of our study required a control and a case group based on standard definitions about the presence or absence of glaucoma. Although these have been widely accepted and applied to most clinical diagnostic studies in the disease, it is difficult to properly establish an appropriate cut-off to separate healthy from glaucomatous subjects with current available reference standard tests. However, by calculating likelihood ratios for continuous RNFL thicknesses and posttest probabilities, we emphasized the magnitude of abnormality of the diagnostic test result, which helps overcome some limitations of the potentially artificial categorization of subjects into diseased vs nondiseased groups.

In conclusion, the methodology enabled calculation of continuous likelihood ratio values for specific global RNFL thickness measurements provided by the Spectralis. Our results can be used to provide a more accurate estimation of the posttest probability of disease by incorporating likelihood ratios for continuous RNFL thicknesses into the diagnostic process with the help of the modified Fagan nomogram. The methodology can also be easily extended to calculation of continuous likelihood ratio values for other instruments and can potentially facilitate the incorporation of results of diagnostic tests into clinical decision making in glaucoma.

ALL AUTHORS HAVE COMPLETED AND SUBMITTED THE ICMJE FORM FOR DISCLOSURE OF POTENTIAL CONFLICTS OF INTEREST and the following were reported: Kaweh Mansouri: consultancy to Sensimed Aktien Gesellschaft; Linda M. Zangwill: research equipment provided by Carl Zeiss and Heildelberg; Robert N. Weinreb: consultancy to Optovue, Nidek, Topcon, and Meditec; and grants from Novartis, Nidek, Topcon, and Aeris; Felipe A. Medeiros: grants from Carl-Zeiss Meditec and Heildelberg Engineering. Funding support was provided by Coordenação de Aperfeiçoamento de Pessoal de Nível Superior grant Bolsas no Exterior 1066/11-0, Brazil (Renato Lisboa); National Eye Institute grant EY021818 (Felipe A. Medeiros) and EY11008 (Linda M. Zangwill); unrestricted grant from Research to Prevent Blindness (New York, NY); grant for participants' glaucoma medications from Alcon, Allergan, Pfizer, Merck, and Santen. Contributions of authors: design and conduct of the study (R.L., K.M., L.M.Z., R.N.W., F.A.M.); analysis and interpretation (R.L., F.A.M.); writing the article (R.L., F.A.M.); critical revision of the article (R.L., K.M., L.M.Z., R.N.W., F.A.M.); final approval of the article (R.L., K.M., L.M.Z., R.N.W., F.A.M.); data collection (R.L., L.M.Z., R.N.W., F.A.M.); provision of material and patient resources (L.M.Z., R.N.W., F.A.M.); statistical expertise (R.L., F.A.M.); obtaining funding (L.M.Z., R.N.W., F.A.M.); literature search (R.L., F.A.M.); and administrative, technical, or logistic support (L.M.Z., R.N.W., F.A.M.).

REFERENCES

1. Jaeschke R, Guyatt GH, Sackett DL. Users' guides to the medical literature. III. How to use an article about a diagnostic test. B. What are the results and will they help me in caring for my patients? The Evidence-Based Medicine Working Group. *JAMA* 1994;271(9):703–707.
2. Medeiros FA, Zangwill LM, Bowd C, Weinreb RN. Comparison of the GDx VCC scanning laser polarimeter, HRT II confocal scanning laser ophthalmoscope, and stratus OCT optical coherence tomograph for the detection of glaucoma. *Arch Ophthalmol* 2004;122(6):827–837.
3. Medeiros FA, Zangwill LM, Bowd C, Sample PA, Weinreb RN. Use of progressive glaucomatous optic disk change as the reference standard for evaluation of diagnostic tests in glaucoma. *Am J Ophthalmol* 2005;139(6):1010–1018.
4. Garas A, Vargha P, Hollo G. Diagnostic accuracy of nerve fibre layer, macular thickness and optic disc measurements made with the RTVue-100 optical coherence tomograph to detect glaucoma. *Eye (Lond)* 2011;25(1):57–65.
5. Li G, Fansi AK, Boivin JF, Joseph L, Harasymowycz P. Screening for glaucoma in high-risk populations using optical coherence tomography. *Ophthalmology* 2010;117(3):453–461.
6. Tandberg D, Deely JJ, O'Malley AJ. Generalized likelihood ratios for quantitative diagnostic test scores. *Am J Emerg Med* 1997;15(7):694–699.
7. Sonis J. How to use and interpret interval likelihood ratios. *Fam Med* 1999;31(6):432–437.
8. Fedorov V, Mannino F, Zhang R. Consequences of dichotomization. *Pharm Stat* 2009;8(1):50–61.
9. Hollander N, Sauerbrei W, Schumacher M. Confidence intervals for the effect of a prognostic factor after selection of an 'optimal' cutpoint. *Stat Med* 2004;23(11):1701–1713.
10. Royston P, Altman DG, Sauerbrei W. Dichotomizing continuous predictors in multiple regression: a bad idea. *Stat Med* 2006;25(1):127–141.
11. Sample PA, Girkin CA, Zangwill LM, et al. The African Descent and Glaucoma Evaluation Study (ADAGES): design and baseline data. *Arch Ophthalmol* 2009;127(9):1136–1145.
12. Medeiros FA, Ng D, Zangwill LM, Sample PA, Bowd C, Weinreb RN. The effects of study design and spectrum bias on the evaluation of diagnostic accuracy of confocal scanning laser ophthalmoscopy in glaucoma. *Invest Ophthalmol Vis Sci* 2007;48(1):214–222.
13. Medeiros FA, Vizzeri G, Zangwill LM, Alencar LM, Sample PA, Weinreb RN. Comparison of retinal nerve fiber layer and optic disc imaging for diagnosing glaucoma in patients suspected of having the disease. *Ophthalmology* 2008;115(8):1340–1346.
14. Medeiros FA. How should diagnostic tests be evaluated in glaucoma? *Br J Ophthalmol* 2007;91(3):273–274.
15. Lisboa R, Leite MT, Zangwill LM, Tafreshi A, Weinreb RN, Medeiros FA. Diagnosing preperimetric glaucoma with spectral domain optical coherence tomography. *Ophthalmology* 2012;119(11):2261–2269.
16. Lisboa R, Paranhos A Jr, Weinreb RN, Zangwill LM, Leite MT, Medeiros FA. Comparison of different spectral domain OCT scanning protocols for diagnosing preperimetric glaucoma. *Invest Ophthalmol Vis Sci* 2013;54(5):3417–3425.
17. Leite MT, Rao HL, Weinreb RN, et al. Agreement among spectral-domain optical coherence tomography instruments for assessing retinal nerve fiber layer thickness. *Am J Ophthalmol* 2011;151(1):85–92.e1.
18. Leite MT, Rao HL, Zangwill LM, Weinreb RN, Medeiros FA. Comparison of the diagnostic accuracies of the Spectralis, Cirrus, and RTVue optical coherence tomography devices in glaucoma. *Ophthalmology* 2011;118(7):1334–1339.
19. Vizzeri G, Balasubramanian M, Bowd C, Weinreb RN, Medeiros FA, Zangwill LM. Spectral domain-optical coherence tomography to detect localized retinal nerve fiber layer defects in glaucomatous eyes. *Opt Express* 2009;17(5):4004–4018.
20. Leung CK, Ye C, Weinreb RN, et al. Retinal nerve fiber layer imaging with spectral-domain optical coherence tomography a study on diagnostic agreement with Heidelberg Retinal Tomograph. *Ophthalmology* 2010;117(2):267–274.
21. Radack KL, Rouan G, Hedges J. The likelihood ratio. An improved measure for reporting and evaluating diagnostic test results. *Arch Pathol Lab Med* 1986;110(8):689–693.
22. Fagan TJ. Letter: nomogram for Bayes theorem. *N Engl J Med* 1975;293(5):257.
23. Gu W, Pepe MS. Estimating the diagnostic likelihood ratio of a continuous marker. *Biostatistics* 2011;12(1):87–101.
24. Rao HL, Leite MT, Weinreb RN, et al. Effect of disease severity and optic disc size on diagnostic accuracy of RTVue spectral domain optical coherence tomograph in glaucoma. *Invest Ophthalmol Vis Sci* 2011;52(3):1290–1296.
25. Leite MT, Zangwill LM, Weinreb RN, et al. Effect of disease severity on the performance of Cirrus spectral-domain OCT for glaucoma diagnosis. *Invest Ophthalmol Vis Sci* 2010;51(8):4104–4109.
26. Medeiros FA, Sample PA, Zangwill LM, Liebmann JM, Girkin CA, Weinreb RN. A statistical approach to the

evaluation of covariate effects on the receiver operating characteristic curves of diagnostic tests in glaucoma. *Invest Ophthalmol Vis Sci* 2006;47(6):2520–2527.
27. Alonzo TA, Pepe MS. Distribution-free ROC analysis using binary regression techniques. *Biostatistics* 2002;3(3):421–432.
28. Janes H, Pepe MS. Adjusting for covariates in studies of diagnostic, screening, or prognostic markers: an old concept in a new setting. *Am J Epidemiol* 2008;168(1):89–97.
29. Zhou XH, Obuchowski NA, McClish DK. Analysis of correlated ROC data. In: Zhou XH, Obuchowski NA, McClish DK. Statistical Methods in Diagnostic Medicine. New York: Wiley; 2002:274–306.
30. Choi BC. Slopes of a receiver operating characteristic curve and likelihood ratios for a diagnostic test. *Am J Epidemiol* 1998;148(11):1127–1132.
31. Pepe MS, Cai T. The analysis of placement values for evaluating discriminatory measures. *Biometrics* 2004;60(2):528–535.
32. Wang X, Li S, Fu J, et al. Comparative study of retinal nerve fibre layer measurement by RTVue OCT and GDx VCC. *Br J Ophthalmol* 2011;95(4):509–513.
33. Park SB, Sung KR, Kang SY, Kim KR, Kook MS. Comparison of glaucoma diagnostic Capabilities of Cirrus HD and Stratus optical coherence tomography. *Arch Ophthalmol* 2009; 127(12):1603–1609.
34. Chang RT, Knight OJ, Feuer WJ, Budenz DL. Sensitivity and specificity of time-domain versus spectral-domain optical coherence tomography in diagnosing early to moderate glaucoma. *Ophthalmology* 2009;116(12):2294–2299.
35. Leung CK, Cheung CY, Weinreb RN, et al. Retinal nerve fiber layer imaging with spectral-domain optical coherence tomography: a variability and diagnostic performance study. *Ophthalmology* 2009;116(7):1257–1263. 1263.e1–2.
36. Rao HL, Zangwill LM, Weinreb RN, Sample PA, Alencar LM, Medeiros FA. Comparison of different spectral domain optical coherence tomography scanning areas for glaucoma diagnosis. *Ophthalmology* 2010;117(9):1692–1699. 1699.e1.
37. Wu H, de Boer JF, Chen TC. Diagnostic capability of spectral-domain optical coherence tomography for glaucoma. *Am J Ophthalmol* 2012;153(5):815–826.e2.
38. Bowd C, Chan K, Zangwill LM, et al. Comparing neural networks and linear discriminant functions for glaucoma detection using confocal scanning laser ophthalmoscopy of the optic disc. *Invest Ophthalmol Vis Sci* 2002;43(11):3444–3454.

APPENDIX: MATHEMATICAL DERIVATION OF LIKELIHOOD RATIO FROM THE ROC CURVE

USING A THRESHOLD C, A CONTINUOUS TEST RESULT Y CAN BE defined as test positive if $Y \geq c$ or test negative if $Y < c$. The ROC curve is the entire set of possible true- and false-positive fractions attainable by dichotomizing Y with different thresholds c_i. The likelihood function is mathematically related to the ROC curve. The ROC curve, ROC(q), where q denotes the false-positive rate, can be interpreted as the probability that a diseased individual has test results Y_D that are greater than or equal to the qth quantile of the distribution of tests results from nondiseased individuals. That is, if the specificity of the test is $1-q$ at a threshold c, the sensitivity is ROC(q).[24–26] The classic ROC model can be written as:

$$\mathrm{ROC}(q) = \Phi\left[\theta_0 + \theta_1 \Phi^{-1}(q)\right]$$

where Φ represents the normal cumulative distribution function, Φ^{-1} represents the inverse normal cumulative distribution function, and the coefficients θ_0 and θ_1 correspond to the intercept and the slope of the ROC curve. The coefficients of the ROC curve can be estimated using the distribution-free binary regression algorithm described by Alonzo and Pepe.[27] This model is able to adjust for the differences in age and sex between control and cases by fitting a linear regression of the marker distribution on the adjustment variables among controls. Standardized residuals based on the fitted linear model are used in place of the marker values for cases and controls.[28] This ROC model is also able to adjust for the potential correlation between eyes by considering the cluster of the data for the study subject when resampling for the calculation of standard errors.[27,29]

The likelihood ratio can be defined as the tangent of the ROC curve at the threshold c corresponding to the point [q, ROC(q)] (Supplemental Figure 2, available at AJO.com).[30] The corresponding estimator of likelihood ratio, LR(y), can be written as:

$$\mathrm{LR}(y) = \theta_1 \varphi\left\{\theta_0 + \theta_1 \Phi^{-1}[\mathrm{U}(y)]\right\} / \varphi\left\{\Phi^{-1}[\mathrm{U}(y)]\right\}$$

where φ represents the probability density function. $U(y)$ stands for the placement value, which represents the proportion of controls with marker measurements at least as large as y and is simply a transformation of Y that standardizes it to the distribution in the control group.[31] An estimate of $U(y)$ is $\hat{U}(y) = 1\text{-}F_C(y)$, where $F_C(y)$ is the empirical cumulative distribution function of Y in the controls.

After adjustment for differences in age and sex between groups, the coefficients θ_0 and θ_1 (with 95% confidence interval) of the ROC curve were estimated at −1.45 (95% CI: −1.79 to −1.14) and 0.71 (95% CI: 0.51 to 0.91), resulting in the following final model for calculating likelihood ratios for continuous global RNFL thickness values, LR(*mfl*):

$$\mathrm{LR}(\mathrm{rnfl}) = 0.71\varphi\{-1.45 + 0.71\Phi^{-1}[\mathrm{U}(\mathrm{rnfl})]\} / \varphi\{\Phi - 1[\mathrm{U}(\mathrm{rnfl})]\}$$

with $U(mfl)$ estimated by 1-Φ[(rnfl-97)/10] and *mfl* corresponding to the RNFL thickness measurement.

The model showed adequate fit to the data, with identical areas under the empirical and modeled ROC curves (0.88).

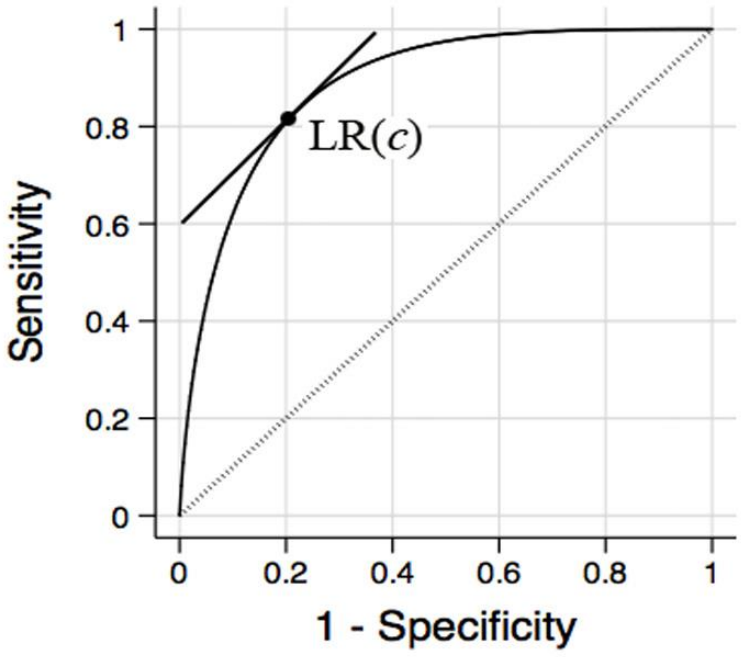

Supplemental Figure 1

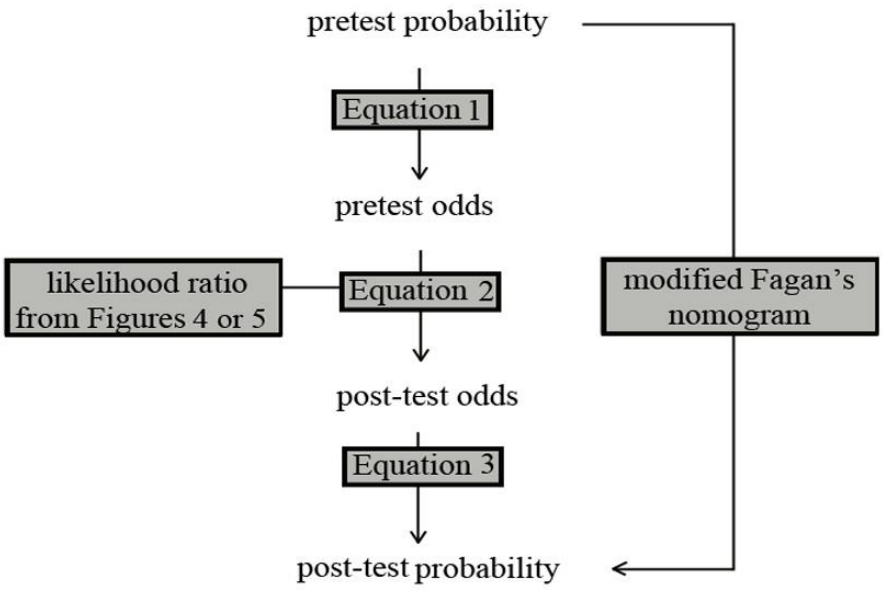

Supplemental Figure 2

3. DISCUSSÃO

"It's a long way to wisdom, but it's a short one to be ignored."

The Lumineers
Banda americana de folk rock

Os estudos aqui apresentados avaliaram a capacidade do SD-OCT detectar o dano estrutural glaucomatoso em um contexto que se assemelha àquele encontrado na prática clínica. Também foi possível calcular razões de verossimilhança para valores contínuos da espessura da CFNR e consequentemente propor um nomograma de Fagan modificado que pode ser utilizado na prática clínica para calcular a probabilidade pós-teste da doença a partir da probabilidade pré-teste da doença e do resultado da espessura da CFNR.

Diversos estudos anteriores avaliaram a capacidade diagnóstica do SD-OCT detectar o dano glaucomatoso.[18,22,23,26] Seus autores utilizaram a existência de defeito no campo visual como referência para essa classificação. Isto é, os pacientes foram selecionados com base na detecção de dano campimétrico reprodutível, enquanto os indivíduos do grupo controle não deveriam apresentar dano campimétrico, tampouco aparência suspeita para glaucoma da CNO. Estes estudos são importantes por possibilitar uma avaliação inicial da capacidade diagnóstica dos instrumentos em questão. Ou seja, se essa tecnologia não for capaz de diferenciar pacientes com achados típicos da doença de indivíduos sadios, ela será considerada inapropriada para fins diagnósticos. Contudo, vale ressaltar, se o instrumento for eficaz nesta fase, ainda serão necessárias novas avaliações para confirmar se ele é capaz de agregar informação relevante em uma situação de incerteza diagnóstica semelhante à encontrada na prática clínica. Ressalte-se, ainda, que a presença de dano glaucomatoso reprodutível no campo visual torna desnecessária a realização de exames de imagens onerosos com a finalidade diagnóstica.

Para avaliar a capacidade diagnóstica do SD-OCT em uma população que se assemelhe àquela encontrada na prática clínica, incluimos nos três

estudos aqui apresentados uma coorte de pacientes suspeitos de glaucoma. Todos apresentavam dano estrutural da CNO na sua avaliação inicial, como afinamento localizado da rima neural, aumento da relação copa/disco ou defeito na CFNR. Estes pacientes apresentavam também campo visual normal durante todo o acompanhamento até a realização dos exames de imagem. A diferenciação destes pacientes em glaucomatosos ou controles só foi possível atravéz do acompanhamento seriado com estereofotografias da CNO. Aqueles que apresentaram dano estrutural documentado em estereofotografias foram classificados como portadores de glaucoma pré-perimétrico, enquanto os que mantiveram uma aparência estável da CNO foram classificados como controles.

No último estudo aqui apresentado foram incluídos, além de os pacientes suspeitos de glaucoma, os indivíduos sadios, bem como os pacientes com dano glaucomatoso perimétrico. Os indivíduos sadios apresentavam aparência fisiológica da CNO e campos visuais normais, ao passo que pacientes com glaucoma perimétrico apresentavam campo visual alterado, independentemente da aparência da CNO. A inclusão destes três grupos de pacientes foi necessária para estimar razões de verossimilhança para o maior intervalo possível de valores de espessura da CFNR.

No primeiro estudo apresentado nesta tese avaliamos a capacidade do SD-OCT detectar dano glaucomatoso pré-perimétrico. A espessura da CFNR fornecida por ele teve melhor performance que o oftalmoscópio confocal de varredura a laser. Nossos achados estão de acordo com os resultados publicados por Leung *et al.*,[23] em que o SD-OCT apresentou melhor habilidade para diferenciar pacientes com dano perimétrico de indivíduos sadios. A melhor capacidade diagnóstica do SD-OCT na nossa coorte de pacientes suspeitos de glaucoma pode ser justificada pela forma como os pacientes foram selecionados. Apenas pacientes com aparência suspeita da CNO para glaucoma foram incluídos no nosso estudo. Sendo assim é de se esperar que a avaliação topográfica da CNO agregue pouca informação diagnóstica, uma vez que tanto grupos controle como pacientes com glaucoma pré-perimétrico apresentavam características parecidas da CNO à biomicroscopia. Por outro lado, a avaliação

da CFNR forneceu informação mais valiosa na detecção de dano glaucomatoso pré-perimétrico.

É importante ressaltar que as áreas abaixo das curvas ROC reportadas no primeiro estudo desta tese foram consideravelmente inferiores àquelas reportadas por Leung *et al.*[23] Enquanto estes autores observaram áreas abaixo da curva ROC de 0.978 para o parâmetro espessura média da CFNR, nós encontramos uma área abaixo da curva ROC de 0.860 para o mesmo parâmetro. Isto pode ser explicado pelo estágio menos avançado da doença dos pacientes identificados como portadores de glaucoma pré-perimétrico em nosso estudo. Leite *et al.*[37] mostraram que a área abaixo da curva ROC depende da gravidade da doença dos pacientes incluídos no grupo de casos. Quanto mais avançada a doença maiores são as áreas abaixo das curvas ROC. Por não apresentar dano perimétrico, os pacientes incluídos no nosso grupo de casos encontravam-se em um estágio mais precoce da doença, dificultando assim sua diferenciação dos indivíduos incluídos no grupo controle.

Além disso, as menores áreas abaixo da curva ROC reportadas em nosso estudo estão relacionadas com os critérios de seleção dos olhos incluídos no grupo controle, já que estes também tinham aparência suspeita da CNO. Isto fez com que, mais uma vez, o teste diagnóstico apresentasse maior dificuldade em diferenciar os controles dos pacientes com glaucoma.

Em um estudo recente realizado por Rao *et al.,*[38] os autores avaliaram a capacidade do SD-OCT diferenciar pacientes com dano glaucomatoso inicial de dois grupos controle distintos. O primeiro grupo controle era composto por indivíduos saudáveis que procuraram uma consulta de rotina. O segundo grupo controle era composto por indivíduos que foram identificados por oftalmologistas gerais como possuidores de glaucoma. Estes apresentavam uma aparência suspeita do disco óptico, mas após serem avaliados por especiaistas em glaucoma foram classificados como saudáveis. Quando o primeiro grupo foi incluído na análise estatística, as áreas abaixo da curva ROC foram semelhantes àquelas reportadas por estudos anteriores.[15,20,23,24] Contrariamente,

quando o segundo grupo controle foi utilizado, as áreas abaixo da curva ROC reportadas foram consideravelmente inferiores.

Após concluírmos que a avaliação da CFNR fornecida pelo SD-OCT apresenta melhor capacidade diagnóstica do que a avaliação topográfica fornecida pelo oftalmoscópio de varredura a laser, avaliamos a capacidade diagnóstica de diferentes protocolos fornecidos pelo SD-OCT em pacientes suspeitos de glaucoma. Utilizando a mesma coorte do primeiro estudo, comparamos, em um segundo estudo, parâmetros que avaliam a espessura da CFNR, a topografia da CNO e a espessura macular fornecidos pelo SD-OCT. Mais uma vez, parâmetros relacionados com a espessura da CFNR apresentaram maiores áreas abaixo das curvas ROC.

A pior capacidade diagnóstica de parâmetros topográficos da CNO reportados no segundo estudo pode refletir a incapacidade do software detectar danos topográficos. A avaliação topografica da CNO fornecida pelo SD-OCT usa um plano de referência 150 μm acima do epitélio pigmentado da retina para definir a transição entre escavação e rima, não levando em consideração a variabilidade normal da CNO na população saudável. Isto dificulta a avaliação pelo software de CNOs planas e tiltadas, por exemplo. Além disso, apesar de todas as imagens terem sido revisadas, este protocolo ainda está sujeito a erro humano, uma vez que a delineação manual e a centralização da CNO pode ser necessária. Por outro lado, o algoritmo da CFNR não depende de um plano de referência e é menos suscetível à influência de variações do fenótipo normal.

Zeimer *et al.*[39] foram os primeiros a sugerir que medidas maculares poderiam ser úteis para o diagnóstico de glaucoma. Após este estudo vários outros foram realizados para testar a efetividade de tais medidas na detecção do dano glaucomatoso.[22,40-46] Teoricamente, parâmetros maculares têm algumas vantagens sobre os parâmentros que avaliam a CFNR para o diagnóstico de glaucoma. A mácula tem a maior concentração de células ganglionares na retina e, consequentemente, a diminuição destas células poderia ser mais precocemente detectada. De fato, alguns estudos relataram que medidas maculares são similares ou até mesmo discretamente melhores do que medidas

da CFNR para o diagnóstico de glaucoma.[40,44-46] Contudo os resultados apresentados no nosso segundo estudo não mostram a mesma tendência. A melhor capacidade diagnóstica macular reportada por outros estudos pode ser também explicada pelo grau de gravidade da doença dos pacientes incluídos nesses estudos. No glaucoma avançado, a mácula tem maior chance de estar comprometida e medidas nesta região serão provavelmente capazes de detectar dano estrutural. Porém, nos casos de glaucoma pré-perimétrico incluídos nesta tese é provável que a mácula ainda esteja intacta e que alterações no campo visual sejam imperceptíveis.

Outra possível explicação para a performance inferior dos parâmetros maculares está na forma como é definido o complexo de células ganglionares pelo software disponível no RTVue. Este software é incapaz de diferenciar a camada de células ganglionares da CFNR e da membrana limitante interna. Uma vez que fibras nervosas de áreas remotas da retina cruzam a área dos escans maculares, a espessura da camada de células ganglionares em uma determinada região pode incorporar CFNRs que não correspondem à área escaneada. É possível que algoritmos de segmentação que incluam apenas o corpo das células ganglionares apresentem melhor capacidade diagnóstica quando comparados ao algoritmo atualmente disponível no RTVue.

Apesar de os parâmetros topográficos e maculares fornecidos pelo SD-OCT terem apresentado performance inferior aos da CFNR em nosso segundo estudo, deve-se salientar que é possível que informações fornecidas por eles melhore a capacidade diagnóstica do aparelho quando combinada às informações fornecidas pelas medidas da CFNR. Medeiros *et al.*[12] estudaram a acurácia diagnóstica do TD-OCT e demonstraram que a informação combinada de parâmetros que avaliaram a CFNR, a topografia da CNO e a espessura macular obteve acurácia diagnóstica superior àquela apresentada por parâmetros isolados.

Em outro estudo realizado por Medeiros *et al*.,[47] os autores avaliaram a capacidade de diferentes parâmetros do TD-OCT diferenciar progressores de não progressores. Os autores reportaram, mais uma vez, uma superioridade das

medidas da CFNR. Vale ressaltar que a metodologia aplicada por aqueles autores foi semelhante à apresentada nos dois primeiros estudos incluídos nesta tese, apesar de os exames serem distintos. No estudo de Medeiros *et al.*[47] foram incluídos pacientes suspeitos de glaucoma e com diagnóstico estabelecido de glaucoma na avaliação inicial. Foram ainda considerados progressores aqueles que apresentaram dano glaucomatoso progressivo em campos visuais ou em estereofotografias seriadas. Em nossos estudos, por outro lado, foram incluídos apenas pacientes que apresentavam suspeita de glaucoma na visita inicial. Mesmo assim, as áreas abaixo da curva ROC para as medidas da espessura média da CFNR reportadas naquele estudo (0.84) foram próximas às reportadas em nosso segundo estudo (0.89).

Finalmente, após concluírmos que a avaliação da espessura da CFNR fornecida pelo SD-OCT é capaz de fornecer maior informação diagnóstica para a avaliação de pacientes suspeitos de glaucoma, realizamos um terceiro estudo em que foram calculadas razões de verossimilhança para valores contínuos da espessura média da CFNR. Apesar da espessura média da CFNR não ter sido o parâmetro que apresentou a melhor capacidade diagnóstica no nosso primeiro estudo, ela foi escolhida para o cálculo de valores contínuos de razões de verossimilhança no terceiro estudo incluído nesta teste, pois apresentou melhor capacidade diagnóstica em estudos publicados previamente na literatura.[21,26] Desta forma a interpretação dos resultados apresentados no terceiro estudo não ficam limitados a pacientes com glaucoma pré-perimétrico e podem ser extrapolados para indivíduos com estágios mais avançados da doença e para aqueles considerados saudáveis. A razão de verossimilhança proporciona uma forma direta de agregar a informação fornecida por um teste diagnóstico na prática clínica diária. Embora as medidas de sensibilidade, especificidade e área abaixo da curva ROC sejam utilizadas rotineiramente em estudos para avaliar a acurácia diagnóstica de instrumentos de imagem em glaucoma,[16,18,19,22,25,26,48] estas medidas têm um significado pouco intuitivo, dificultando sua aplicabilidade para um paciente específico.

O ponto de partida do processo diagnóstico ocorre quando o médico combina história clínica e exame físico com o objetivo de estimar a probabilidade de presença da doença, também conhecida como probabilidade pré-teste. Em seguida os resultados de um exame auxiliar podem ser utilizados para modificar a suspeita inicial de doença em uma probabilidade mais conclusiva, também conhecida como probabilidade pós-teste. A razão de verossimilhança pode ser usada de uma forma prática para derivar a probabilidade pós-teste de doença. Adicionalmente, o nomograma de Fagan modificado, proposto em nosso terceiro estudo, pode ser utilizado diretamente para calcular a probabilidade de glaucoma a partir da probabilidade inicial de doença e das medidas de espessura da CFNR fornecidas pelo SD-OCT. Por exemplo, se a probabilidade de glaucoma pré-teste em um olho suspeito de ter a doença for de 50% e soubermos que a espessura média da CFNR deste mesmo olho é de 75 μm, então, ao aplicar o nomograma de Fagan modificado, encontraremos probabilidade pós-teste de 88% para glaucoma.

Os impressos dos resultados dos SD-OCTs disponibilizam classificações da espessura da CFNR de acordo com comparações com um banco de dados normativo. Apesar de a categorização de resultados contínuos ter o objetivo de simplificar a interpretação dos resultados na prática clínica, esta categorização pode levar a uma importante perda de informação e causar distorção na interpretação dos resultados do teste, uma vez que medidas da espessura da CFNR claramente distintas podem receber o mesmo valor diagnóstico.[32-35] Por exemplo, ao utilizar a abordagem convencional, um médico iria classificar um olho como glaucomatoso se a espessura da CFNR aferida estivesse abaixo do ponto de corte de 1%, calculado a partir da distribuição dos valores de espessura da CFNR no banco de dados normativo. Este tipo de abordagem leva à decisão de "tudo ou nada", ignorando o fato de que pacientes incluídos na mesma categoria podem, na realidade, apresentar probabilidades de doença completamente distintas. Dois olhos com espessura da CFNR de 73 μm e 65 μm iriam ser categorizados como fora dos limites da normalidade pela abordagem convencional, sem nenhuma distinção entre eles, uma vez que ambos estariam

abaixo do limite inferior de 1% encontrado na população sadia (74 μm). Contudo, se considerarmos a mesma probabilidade pré-teste de 30% para ambos os olhos, por exemplo, a aplicação da razão de verossimilhança para valores contínuos da espessura da CFNR levaria a diferentes probabilidades pós-teste de 83% e 97%. A mesma lógica pode ser aplicada para olhos classificados como dentro dos limites da normalidade, utilizando a abordagem convencional.

Apesar de os métodos aqui demonstrados para o cálculo de razões de verossimilhança para valores contínuos da espessura da CFNR exigirem conhecimento matemático avançado, esse algoritmo pode ser facilmente implementado nos software de exames de imagem. Desta forma, oftalmologistas poderiam ter à sua disposição as razões de verossimilhança associadas com cada valor de espessura da CFNR e facilmente calcular a probabilidade pós-teste da doença.

Os resultados aqui apresentados demonstraram que a avaliação da espessura da CFNR fornecida pelo SD-OCT apresentou capacidade superior para detectar dano glaucomatoso pré-perimétrico, quando comparada com parâmetros maculares e parâmetros topográficos da CNO fornecidos também pelo SD-OCT e pelo CSLO. Demonstraram, também, que razões de verossimilhança puderam ser determinadas para valores contínuos da espessura da CFNR fornecidos pelo SD-OCT. Com a ajuda do nomograma de Fagan modificado, medidas da espessura da CFNR podem ser incorporadas na prática clínica para fornecer uma probabilidade pós-teste mais conclusiva para glaucoma. Assim sendo, consideramos que estes resultados têm uma implicação significativa no uso do SD-OCT para diagnosticar dano glaucomatoso na prática clínica.

4. CONCLUSÕES

1. A espessura da camada de fibras nervosas da retina fornecida pela tomografia de coerência óptica de domínio espectral apresentou boa performance na detecção de dano glaucomatoso pré-perimétrico em pacientes suspeitos de glaucoma, apresentando melhor capacidade diagnóstica que o oftalmoscópio confocal de varredura a laser.

2. A medida da espessura da camada de fibras nervosas da retina fornecida pela tomografia de coerência óptica de domínio espectral apresentou maior capacidade para detectar dano glaucomatoso pré-perimétrico quando comparada a medidas topográficas da cabeça do nervo óptico e da espessura macular fornecidas pelo mesmo instrumento.

3. Razões de verossimilhança puderam ser estimadas para valores contínuos da espessura da camada de fibras nervosas da retina, fornecidas pela tomografia de coerência óptica de domínio espectral. Os resultados podem ser incorporados à prática clínica com o auxílio do nomograma de Fagan modificado.

Medidas da espessura da camada de fibras nervosas da retina apresentaram boa capacidade em detectar o dano glaucomatoso pré-perimétrico. Estas medidas apresentaram capacidade diagnóstica superior a medidas topográficas da cabeça do nervo óptico e medidas da espessura macular. O nomograma de Fagan modificado pode ser utilizado para agregar a informação fornecida pelo SD-OCT no processo diagnóstico em glaucoma.

5. ANEXOS

5.1. Aprovação do Comitê de Ética em Pesquisa

071153

UNIVERSITY OF CALIFORNIA, SAN DIEGO
HUMAN RESEARCH PROTECTIONS PROGRAM

TO: Linda Zangwill Mailcode: 0946

RE: Project #071153
Diagnostic Innovations in Glaucoma Study (DIGS)

Dear Dr. Zangwill:

The above-referenced project was reviewed and approved by one of this institution's Institutional Review Boards in accordance with the requirements of the Code of Federal Regulations on the Protection of Human Subjects (45 CFR 46 and 21 CFR 50 and 56), including its relevant Subparts. This approval, based on the degree of risk, is for 365 days from the date of **IRB review and approval** unless otherwise stated in this letter. The regulations require that continuing review be conducted on or before the 1-year anniversary date of the IRB approval, even though the research activity may not begin until some time after the IRB has given approval.

The IRB determined that this project presents more than minimal risk to human subjects in that the probability and magnitude of harm or discomfort anticipated in the research are greater in and of themselves than those ordinarily encountered in daily life or during the performance of routine physical or psychological examinations or tests. **Date of IRB review and approval**: **2/7/2013**

On behalf of the Institutional Review Board,

/mb
Michael Caligiuri, Ph.D.
Director, Human Research Protections Program
(858) 657-5100

Note: All Human Subject research conducted at the VA facility and/or utilizing VA/VMRF funds MUST BE APPROVED by the VA Research and Development Committee prior to commencing any research. In addition, please ensure that the clinical trial agreement or other funding is appropriately in place prior to conducting any research activities.

IRB approval does not constitute funding **or other institutional required approvals.** Should your studies involve other review committees such as Conflict of Interest (COI), Protocol Review Monitoring Committee (PRMC), and committees under Environmental Health & Safety (EH&S) such as Institutional Biosafety Committee (IBC), Human Exposure Committee (HERC), and RSSC (Radiation Safety and Surveillance Committee), it is the researchers responsibility to ensure that all approvals are in place prior to conducting research involving human subjects or their related specimens.

Approval release date: 2/8/2013

5.2. Referências Bibliográficas

1. Susanna Jr R, Weinreb RN. Glaucoma, Perguntas & Respostas. 1ª ed. Rio de Janeiro, RJ, Brasil; 2005: 1-8

2. Foster PJ. The epidemiology of primary angle closure and associated glaucomatous optic neuropathy. *Semin. Ophthalmol.* Jun 2002;17(2):50-58.

3. Medeiros FA, Vizzeri G, Zangwill LM, Alencar LM, Sample PA, Weinreb RN. Comparison of retinal nerve fiber layer and optic disc imaging for diagnosing glaucoma in patients suspected of having the disease. *Ophthalmology.* Aug 2008;115(8):1340-1346.

4. Nassif N, Cense B, Park B*, et al.* In vivo high-resolution video-rate spectral-domain optical coherence tomography of the human retina and optic nerve. *Opt. Express. .* Feb 9 2004;12(3):367-376.

5. Wojtkowski M, Srinivasan V, Ko T, Fujimoto J, Kowalczyk A, Duker J. Ultrahigh-resolution, high-speed, Fourier domain optical coherence tomography and methods for dispersion compensation. *Opt. Express. .* May 31 2004;12(11):2404-2422.

6. Schuman JS. Spectral domain optical coherence tomography for glaucoma (an AOS thesis). *Trans. Am. Ophthalmol. Soc.* 2008;106:426-458.

7. Gonzalez-Garcia AO, Vizzeri G, Bowd C, Medeiros FA, Zangwill LM, Weinreb RN. Reproducibility of RTVue retinal nerve fiber layer thickness and optic disc measurements and agreement with Stratus optical coherence tomography measurements. *Am. J. Ophthalmol.* Jun 2009;147(6):1067-1074, 1074 e1061.

8. Mistlberger A, Liebmann JM, Greenfield DS*, et al.* Heidelberg retina tomography and optical coherence tomography in normal, ocular-hypertensive, and glaucomatous eyes. *Ophthalmology.* Oct 1999;106(10):2027-2032.

9. Zangwill LM, Bowd C, Berry CC*, et al.* Discriminating between normal and glaucomatous eyes using the Heidelberg Retina Tomograph, GDx Nerve Fiber Analyzer, and Optical Coherence Tomograph. *Arch. Ophthalmol.* Jul 2001;119(7):985-993.

10. Greaney MJ, Hoffman DC, Garway-Heath DF, Nakla M, Coleman AL, Caprioli J. Comparison of optic nerve imaging methods to distinguish

normal eyes from those with glaucoma. *Invest. Ophthalmol. Vis. Sci.* Jan 2002;43(1):140-145.

11. Medeiros FA, Zangwill LM, Bowd C, Weinreb RN. Comparison of the GDx VCC scanning laser polarimeter, HRT II confocal scanning laser ophthalmoscope, and stratus OCT optical coherence tomograph for the detection of glaucoma. *Arch. Ophthalmol.* Jun 2004;122(6):827-837.

12. Medeiros FA, Zangwill LM, Bowd C, Vessani RM, Susanna R, Jr., Weinreb RN. Evaluation of retinal nerve fiber layer, optic nerve head, and macular thickness measurements for glaucoma detection using optical coherence tomography. *Am. J. Ophthalmol.* Jan 2005;139(1):44-55.

13. Hougaard JL, Heijl A, Bengtsson B. Glaucoma detection by Stratus OCT. *J. Glaucoma.* May 2007;16(3):302-306.

14. Naithani P, Sihota R, Sony P*, et al.* Evaluation of optical coherence tomography and heidelberg retinal tomography parameters in detecting early and moderate glaucoma. *Invest. Ophthalmol. Vis. Sci.* Jul 2007;48(7):3138-3145.

15. Parikh RS, Parikh S, Sekhar GC*, et al.* Diagnostic capability of optical coherence tomography (Stratus OCT 3) in early glaucoma. *Ophthalmology.* Dec 2007;114(12):2238-2243.

16. Leung CK, Cheung CY, Weinreb RN*, et al.* Retinal nerve fiber layer imaging with spectral-domain optical coherence tomography: a variability and diagnostic performance study. *Ophthalmology.* Jul 2009;116(7):1257-1263, 1263 e1251-1252.

17. Sehi M, Grewal DS, Sheets CW, Greenfield DS. Diagnostic ability of Fourier-domain vs time-domain optical coherence tomography for glaucoma detection. *Am. J. Ophthalmol.* Oct 2009;148(4):597-605.

18. Park SB, Sung KR, Kang SY, Kim KR, Kook MS. Comparison of glaucoma diagnostic Capabilities of Cirrus HD and Stratus optical coherence tomography. *Arch. Ophthalmol.* Dec 2009;127(12):1603-1609.

19. Chang RT, Knight OJ, Feuer WJ, Budenz DL. Sensitivity and specificity of time-domain versus spectral-domain optical coherence tomography in diagnosing early to moderate glaucoma. *Ophthalmology.* Dec 2009;116(12):2294-2299.

20. Rao HL, Babu GJ, Sekhar GC. Comparison of the diagnostic capability of the Heidelberg Retina Tomographs 2 and 3 for glaucoma in the Indian population. *Ophthalmology.* Feb 2010;117(2):275-281.

21. Leung CK, Ye C, Weinreb RN*, et al.* Retinal nerve fiber layer imaging with spectral-domain optical coherence tomography a study on diagnostic agreement with Heidelberg Retinal Tomograph. *Ophthalmology.* Feb 2010;117(2):267-274.

22. Rao HL, Zangwill LM, Weinreb RN, Sample PA, Alencar LM, Medeiros FA. Comparison of different spectral domain optical coherence tomography scanning areas for glaucoma diagnosis. *Ophthalmology.* Sep 2010;117(9):1692-1699, 1699 e1691.

23. Leung CK, Lam S, Weinreb RN*, et al.* Retinal nerve fiber layer imaging with spectral-domain optical coherence tomography: analysis of the retinal nerve fiber layer map for glaucoma detection. *Ophthalmology.* Sep 2010;117(9):1684-1691.

24. Jindal S, Dada T, Sreenivas V, Gupta V, Sihota R, Panda A. Comparison of the diagnostic ability of Moorfield's regression analysis and glaucoma probability score using Heidelberg retinal tomograph III in eyes with primary open angle glaucoma. *Indian J. Ophthalmol.* Nov-Dec 2010;58(6):487-492.

25. Wang X, Li S, Fu J*, et al.* Comparative study of retinal nerve fibre layer measurement by RTVue OCT and GDx VCC. *Br. J. Ophthalmol.* Apr 2011;95(4):509-513.

26. Leite MT, Rao HL, Zangwill LM, Weinreb RN, Medeiros FA. Comparison of the diagnostic accuracies of the Spectralis, Cirrus, and RTVue optical coherence tomography devices in glaucoma. *Ophthalmology.* Jul 2011;118(7):1334-1339.

27. Jaeschke R, Guyatt GH, Sackett DL. Users' guides to the medical literature. III. How to use an article about a diagnostic test. B. What are the results and will they help me in caring for my patients? The Evidence-Based Medicine Working Group. *JAMA.* Mar 2 1994;271(9):703-707.

28. Medeiros FA, Zangwill LM, Bowd C, Sample PA, Weinreb RN. Use of progressive glaucomatous optic disk change as the reference standard for evaluation of diagnostic tests in glaucoma. *Am. J. Ophthalmol.* Jun 2005;139(6):1010-1018.

29. Li G, Fansi AK, Boivin JF, Joseph L, Harasymowycz P. Screening for glaucoma in high-risk populations using optical coherence tomography. *Ophthalmology.* Mar 2010;117(3):453-461.

30. Garas A, Vargha P, Hollo G. Diagnostic accuracy of nerve fibre layer, macular thickness and optic disc measurements made with the RTVue-100 optical coherence tomograph to detect glaucoma. *Eye (Lond).* Jan 2011;25(1):57-65.

31. Tandberg D, Deely JJ, O'Malley AJ. Generalized likelihood ratios for quantitative diagnostic test scores. *Am. J. Emerg. Med.* Nov 1997;15(7):694-699.

32. Sonis J. How to use and interpret interval likelihood ratios. *Fam. Med.* Jun 1999;31(6):432-437.

33. Hollander N, Sauerbrei W, Schumacher M. Confidence intervals for the effect of a prognostic factor after selection of an 'optimal' cutpoint. *Stat. Med.* Jun 15 2004;23(11):1701-1713.

34. Royston P, Altman DG, Sauerbrei W. Dichotomizing continuous predictors in multiple regression: a bad idea. *Stat. Med.* Jan 15 2006;25(1):127-141.

35. Fedorov V, Mannino F, Zhang R. Consequences of dichotomization. *Pharm Stat.* Jan-Mar 2009;8(1):50-61.

36. Fagan TJ. Letter: Nomogram for Bayes theorem. *N. Engl. J. Med.* Jul 31 1975;293(5):257.

37. Leite MT, Zangwill LM, Weinreb RN*, et al.* Effect of disease severity on the performance of Cirrus spectral-domain OCT for glaucoma diagnosis. *Invest. Ophthalmol. Vis. Sci.* Aug 2010;51(8):4104-4109.

38. Rao HL, Kumbar T, Addepalli UK*, et al.* Effect of spectrum bias on the diagnostic accuracy of spectral-domain optical coherence tomography in glaucoma. *Invest. Ophthalmol. Vis. Sci.* Feb 2012;53(2):1058-1065.

39. Zeimer R, Asrani S, Zou S, Quigley H, Jampel H. Quantitative detection of glaucomatous damage at the posterior pole by retinal thickness mapping. A pilot study. *Ophthalmology.* Feb 1998;105(2):224-231.

40. Leung CK, Chan WM, Yung WH*, et al.* Comparison of macular and peripapillary measurements for the detection of glaucoma: an optical coherence tomography study. *Ophthalmology.* Mar 2005;112(3):391-400.

41. Ishikawa H, Stein DM, Wollstein G, Beaton S, Fujimoto JG, Schuman JS. Macular segmentation with optical coherence tomography. *Invest. Ophthalmol. Vis. Sci.* Jun 2005;46(6):2012-2017.

42. Ojima T, Tanabe T, Hangai M, Yu S, Morishita S, Yoshimura N. Measurement of retinal nerve fiber layer thickness and macular volume for glaucoma detection using optical coherence tomography. *Jpn. J. Ophthalmol.* May-Jun 2007;51(3):197-203.

43. Tan O, Li G, Lu AT, Varma R, Huang D. Mapping of macular substructures with optical coherence tomography for glaucoma diagnosis. *Ophthalmology.* Jun 2008;115(6):949-956.

44. Seong M, Sung KR, Choi EH*, et al.* Macular and peripapillary retinal nerve fiber layer measurements by spectral domain optical coherence tomography in normal-tension glaucoma. *Invest. Ophthalmol. Vis. Sci.* Mar 2010;51(3):1446-1452.

45. Moreno PA, Konno B, Lima VC*, et al.* Spectral-domain optical coherence tomography for early glaucoma assessment: analysis of macular ganglion cell complex versus peripapillary retinal nerve fiber layer. *Canadian journal of ophthalmology. Journal canadien d'ophtalmologie.* Dec 2011;46(6):543-547.

46. Nakatani Y, Higashide T, Ohkubo S, Takeda H, Sugiyama K. Evaluation of macular thickness and peripapillary retinal nerve fiber layer thickness for detection of early glaucoma using spectral domain optical coherence tomography. *J. Glaucoma.* Apr-May 2011;20(4):252-259.

47. Medeiros FA, Zangwill LM, Alencar LM*, et al.* Detection of glaucoma progression with stratus OCT retinal nerve fiber layer, optic nerve head, and macular thickness measurements. *Invest. Ophthalmol. Vis. Sci.* Dec 2009;50(12):5741-5748.

48. Wu H, de Boer JF, Chen TC. Diagnostic capability of spectral-domain optical coherence tomography for glaucoma. *Am. J. Ophthalmol.* May 2012;153(5):815-826 e812.